ChemPubSoc Europe

DOI: 10.1002/cmdc.201300218

Chemical, Pharmacological, and in vitro Metabolic Stability Studies on Enantiomerically Pure RC-33 Compounds: Promising Neuroprotective Agents Acting as σ_1 Receptor Agonists

Daniela Rossi,[a] Alice Pedrali,[a] Raffaella Gaggeri,[a] Annamaria Marra,[a] Luca Pignataro,[b] Erik Laurini,[c] Valentina Dal Col,[c] Maurizio Fermeglia,[c] Sabrina Pricl,*[c, d] Dirk Schepmann,[e] Bernhard Wünsch,[e] Marco Peviani,[f] Daniela Curti,[f] and Simona Collina*[a]

Our recent research efforts identified racemic RC-33 as a potent and metabolically stable σ_1 receptor agonist. Herein we describe the isolation of pure RC-33 enantiomers by chiral chromatography, assignment of their absolute configuration, and in vitro biological studies in order to address the role of chirality in the biological activity of these compounds and their metabolic processing. The binding of enantiopure RC-33 to the σ_1 receptor was also investigated in silico by molecular dynamics simulations. Both RC-33 enantiomers showed similar affinities for the σ_1 receptor and appeared to be almost equally effective as σ_1 receptor agonists. However, the *R*-configured enantiomer showed higher in vitro hepatic metabolic stability in the presence of NADPH than the *S* enantiomer. Overall, the results presented herein led us to select (*R*)-RC-33 as the optimal candidate for further in vivo studies in an animal model of amyotrophic lateral sclerosis.

Introduction

Over the last 10 years our research group has conducted extensive studies aimed at discovering novel σ_1 receptor ligands as potential neuroprotective agents.[1] The σ receptor system includes two subtypes: σ_1 and σ_2. The σ_2 subtype seems to be involved mainly in death signaling of cancer cells.[2] Published evidence suggests involvement of the σ_1 receptor in such conditions as drug addiction, depression, neurodegeneration, pain-related disorders, and cancer.[2a] Interestingly, a mutation in the σ_1 receptor gene was recently found to be associated with frontotemporal lobar degeneration (FTLD), which is the most common cause of dementia under age 65,[3] with associated motor neuron disorders and familial juvenile amyotrophic lateral sclerosis (ALS).[4] Additionally, the σ_1 receptor has been implicated in neurite sprouting and elongation in vitro, suggesting a role for this protein in neuroplasticity.[5] Accordingly, the identification of new, potent, and highly selective σ_1 agonists is of significant interest, not only for a better understanding of the role played by σ_1 receptors in various pathologies, but also, as a more challenging task, to develop neuroprotective agents representing an innovative pharmacological approach for the treatment and prevention of neurodegenerative diseases. In this context, our recent efforts have been addressed to the design, synthesis, and biological investigation of new σ_1 receptor ligands based on arylalkenylamine and arylalkylamine scaffolds (Figure 1).[1]

Among our compound library, the most promising molecule is 1-[3-(1,1′-biphen)-4-yl]butylpiperidine hydrochloride (RC-33·HCl, Figure 1), showing excellent σ_1 receptor affinity ($K_i = 0.70 \pm 0.3$ nM) along with high selectivity over the σ_2 subtype, μ- and κ-opioid receptors, and the PCP binding site of NMDA receptors.[1c] RC-33·HCl also turned out to be a potent σ_1 receptor agonist in our validated PC12 cell model of neuronal differentiation. Indeed, this molecule is able to potentiate both nerve growth factor (NGF)-induced neurite outgrowth and elongation in the absence of toxic effects and at lower doses than the well-characterized σ_1 receptor agonist PRE-084.[1c] Finally, RC-33·HCl was found to be metabolically stable in several biological matrices such as mouse and rat blood, and rat,

[a] Dr. D. Rossi, Dr. A. Pedrali, Dr. R. Gaggeri, Dr. A. Marra, Prof. S. Collina
Department of Drug Sciences
Medicinal Chemistry and Pharmaceutical Technology Section
University of Pavia, Viale Taramelli 12, 27100 Pavia (Italy)
E-mail: simona.collina@unipv.it

[b] Dr. L. Pignataro
Dipartimento di Chimica, Università degli Studi di Milano
Istituto di Scienze e Tecnologie Molecolari (ISTM) del CNR
Via Golgi 19, 20133 Milan (Italy)

[c] Dr. E. Laurini, Dr. V. Dal Col, Prof. M. Fermeglia, Prof. S. Pricl
MOSE-DEA, University of Trieste, Via Valerio 10, 34127 Trieste (Italy)
E-mail: sabrina.pricl@di3.units.it

[d] Prof. S. Pricl
National Interuniversity Consortium for Material Science and Technology (INSTM), Research Unit MOSE-DEA, University of Trieste, Trieste (Italy)

[e] Dr. D. Schepmann, Prof. B. Wünsch
Institute of Pharmaceutical and Medicinal Chemistry
University of Muenster, Corrensstrasse 48, 48149 Münster (Germany)

[f] Dr. M. Peviani, Dr. D. Curti
Department of Biology and Biotechnology "L. Spallanzani"
Laboratory of Cellular and Molecular Neuropharmacology
University of Pavia, Via Ferrata 9, 27100 Pavia (Italy)

Supporting information for this article is available on the WWW under http://dx.doi.org/10.1002/cmdc.201300218.

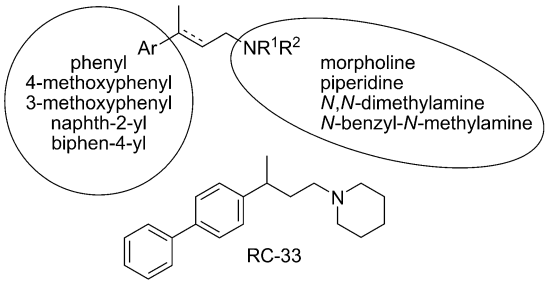

Figure 1. Structures of arylalkenylamines, arylalkylamines, and the most promising compound, RC-33.

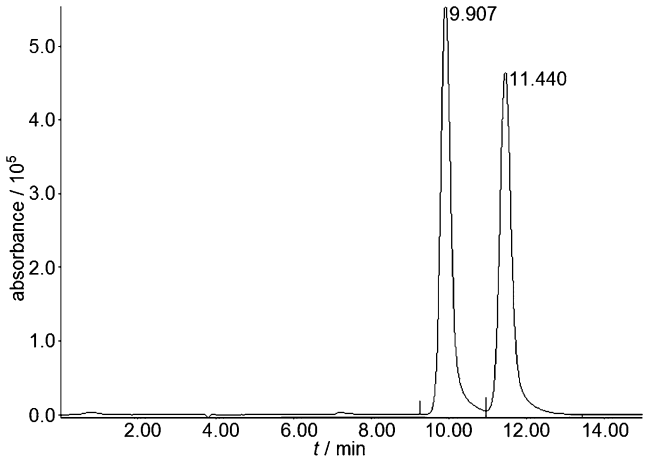

Figure 2. Analytical separation of RC-33 on a Chiralcel OJ-H column ($\varnothing = 0.46$ cm, $l = 15$ cm, 5 μm). Mobile phase: CH_3OH/Et_3N 100:0.1; flow rate: 0.5 mL min^{-1}; detection at $\lambda = 250$ nm.

dog and human plasma. Significant degradation was only observed in rat and human liver S9 fractions in the presence of NADPH.[1d] According to these results, we identified RC-33·HCl as an optimal candidate for the hit-to-lead process. Because the enantiomers of a chiral biologically active molecule may behave differently under physiological conditions (i.e., they can exhibit different pharmacological and/or toxicological profiles), the investigation of enantiopure forms is a key step in the drug discovery and development processes.[6] Accordingly, in the present work we directed our efforts toward investigating the role of chirality in the biological activity and metabolic processing of RC-33. To this end, we isolated the pure enantiomers of RC-33 by chiral chromatography and carried out the assignment of their absolute configuration. The binding of enantiopure RC-33 at the σ_1 receptor was then investigated both in silico, by molecular dynamics (MD) simulations using our recently developed homology model for the σ_1 receptor,[7] and in vitro, by competition experiments with radioligand. The in vitro binding affinities of RC-33 enantiomers for opioid receptors and the PCP binding site of the NMDA receptor were also investigated, together with their capacity to promote NGF-induced neurite outgrowth in PC12 cells. As the last step in the present hit-to-lead process, both RC-33 enantiomers underwent toxicity and in vitro metabolic studies.

Results and Discussion

RC-33 enantiomer isolation and assignment of configuration

Because chiral HPLC is a rapid and efficient method for directly obtaining both enantiomers with high optical purity, the resolution of racemic RC-33 by semi-preparative HPLC using chiral stationary phases (CSPs) was performed to isolate each enantiomer in quantities suitable for in-depth investigations of biological behavior. Firstly, the racemic compound was synthesized via catalytic reduction of the corresponding arylalkenylamine under a hydrogen atmosphere using Pd^0 EnCat 30NP as catalyst.[1c] A standard screening protocol was then applied to an analytical Chiralcel OJ-H column, the chiral selector of which is cellulose tris-(4-methylbenzoate) coated on a silica gel substrate.[8] As shown in Figure 2, baseline separation of RC-33 enantiomers was achieved by eluting with methanol/diethylamine 100:0.1 ($t_{R1} = 9.91$ min; $t_{R2} = 11.44$ min; $\alpha = 1.25$; $R_S = 1.58$). Hence, these experimental conditions were selected for the chromatographic scale-up. Briefly, RC-33 (62.5 mg) was processed in 50 cycles according to conditions reported in Table 1, yielding 26.4 mg of the first eluted enantiomer and 27.8 mg of the second eluted enantiomer, together with 5.2 mg of an intermediate fraction as a mixture of the two enantiomers.

Table 1. Semi-preparative resolution of compound RC-33 on a Chiralcel OJ-H column ($\varnothing = 1$ cm, $l = 25$ cm, 5 μm).

CH_3OH/Et_3N	Flow rate [mL min^{-1}]	t_{R1} [min]	t_{R2} [min]	Inj. Vol. [mL]	Conc. [mg mL^{-1}]
100:0.1	3	11.6	13.0	1	1.25

To approach the configurational study of enantiopure RC-33, an enantioselective synthetic procedure suitable to obtaining enantioenriched RC-33 with known absolute configuration was devised (Scheme 1). As highlighted in Scheme 1, the enantioselective hydrogenation of (*E*)-**1** using (*R*,*R*)-Ir(ThrePHOX) complex as catalyst is the key step of the synthetic pathway. The enantioselective hydrogenation of (*E*)-**2** was also performed as a reference reaction for configurational assignment purposes. Thus, we started our synthetic approach with the preparation of (*E*)-**1** and (*E*)-**2**, essentially according to the procedures described by Lemay et al. and Simard-Mercier et al.[9] Compounds (*E*)-**1** and (*E*)-**2** were then subjected to enantioselective hydrogenation in a Parr multireactor (H_2, 70 bar, room temperature) using the (*R*,*R*)-Ir(ThrePHOX) complex as catalyst, yielding compounds (+)-**4** and (+)-**5**. The absolute configuration of the latter compound is known to be *S*.[10] Both compounds were obtained in 87% *ee*, as demonstrated by chiral HPLC analysis (see the Experimental Section below). The configurational assignment of (+)-**4** was performed by comparing its circular dichroism (CD) spectrum with that of (+)-(*S*)-**5**. As expected, both (+)-**4** and (+)-(*S*)-**5** showed a similar positive Cotton

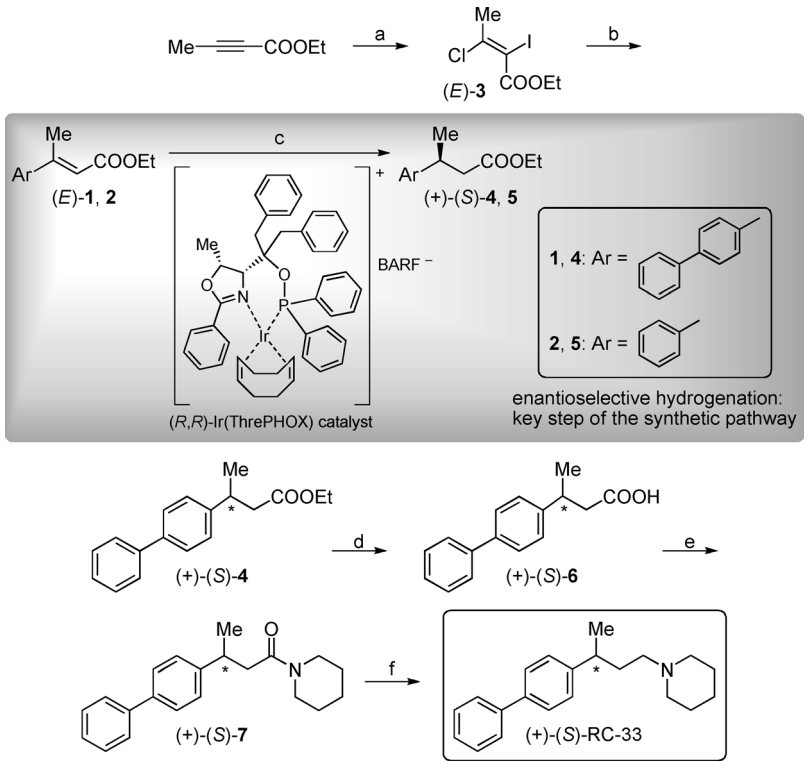

Scheme 1. Synthetic pathway for the preparation of enantiomeric RC-33. *Reagents and conditions*: a) Bu_4NI, DCE, reflux, 24 h; b) arylboronic acid, $Pd_2(dba)_3$, $PtBu_3$ HBF_4, Cs_2CO_3, anhydrous THF, reflux, 4 h; c) H_2 (70 bar), anhydrous CH_2Cl_2, 25 °C, 20 h; d) 2 M NaOH, EtOH, RT, 2 h; e) piperidine, TBTU, DIPEA, THF, MW (80 °C, 25 W, 20 min); f) $LiAlH_4$, anhydrous THF, RT, 3 h.

effect (CE) at ~215 nm (λ_{max} 216, $\Delta\varepsilon_{max}$ 1.13 and λ_{max} 215, $\Delta\varepsilon_{max}$ 1.38 for (+)-**4** and (+)-(*S*)-**5**, respectively). Moreover, compound (+)-**4** exhibited an additional positive CE at higher wavelength (λ_{max} 249, $\Delta\varepsilon_{max}$ 1.73). This behavior is consistent with the compound's UV spectra (Supporting Information). Based on these considerations, the absolute configuration *S* was assigned to (+)-**4**. Compound (+)-(*S*)-**4** was then fully converted, by alkaline hydrolysis, into the corresponding acid (+)-(*S*)-**6** (87% *ee*, determined by chiral HPLC; Experimental Section) which, in turn, was condensed with piperidine in the presence of TBTU to yield the tertiary amide (+)-(*S*)-**7** (87% *ee*, determined by chiral HPLC: Experimental Section). Compound (+)-(*S*)-**7** was finally converted into the desired product (+)-(*S*)-RC-33 (87% *ee*, Table 2) by reduction with lithium aluminum hydride. Importantly, chiral HPLC analysis performed after hydrolysis, amidation, and reduction reactions revealed that no racemization occurs, demonstrating that the *S* configuration was correctly assigned to (+)-RC-33 by chemical correlation to its precursor (+)-(*S*)-**4**. As the final step in the configurational study of enantiopure RC-33 isomers obtained by chiral chromatography, their optical rotation values and retention times from chiral HPLC–UV traces were compared with those of enantioenriched RC-33 obtained by enantioselective synthesis (Table 2). In this way, the *S* configuration was assigned to the first eluted enantiomer, and the *R* configuration to the more retained one. Pure (*R*)- and (*S*)-RC-33 were finally converted into the corresponding hydrochlorides, suitable for biological investigations.

Table 2. Chiroptical properties of RC-33 enantiomers.

Compd	$[\alpha]_D^{20}$ (CH_3OH)	*ee* [%][a]	t_R [min]
(+)-RC-33[b]	+22.1 (*c* = 0.3)	99.5	9.88
(−)-RC-33[b]	−22.2 (*c* = 0.3)	99.6	11.41
(+)-(*S*)-RC-33[c]	+19.2 (*c* = 1)	87.0	9.45 (major) 10.89 (minor)

[a] Determined by chiral HPLC on Chiralcel OJ-H (Figure 2). [b] Obtained by semi-preparative chiral HPLC (Table 1). [c] Obtained by enantioselective synthesis (Scheme 1).

To investigate receptor selectivity, the binding properties of pure RC-33·HCl enantiomers were also investigated for μ-, κ-, δ-opioid receptors and the PCP binding site of NMDA receptors using guinea pig brain (μ and κ), rat brain (δ) and pig brain cortex (PCP binding site of NMDA) as sources of receptor material. [^{3}H]DAMGO (μ), [^{3}H]-U-69,593 (κ), [^{3}H]DPDPE (δ), and [^{3}H]MK-801 (NMDA) were used as specific radioligands. Nonspecific binding was determined with unlabeled naloxone (μ), unlabeled U-69,593 (κ), unlabeled morphine (δ), and unlabeled (+)-MK-801 (PCP binding site of NMDA). The residual binding of the radioligand is given at a test compound concentration of 1 μM (opioid receptor binding assays) or 10 μM (NMDA receptor binding assays). Binding results are summarized in Table 3, together with data for RC-33·HCl, reported for comparison purposes.

The enantiomeric arylalkylamines (*S*)-RC-33·HCl and (*R*)-RC-33·HCl presented herein showed interesting binding properties

Receptor binding studies

The affinities of the pure RC-33·HCl enantiomers for σ_1 and σ_2 receptors were determined in competition experiments with radioligands. The highly σ_1-selective radioligand [^{3}H](+)-pentazocine and homogenates of guinea pig brain cortex were used in the σ_1 assay. Nonspecific binding was recorded in the presence of non-radiolabeled (+)-pentazocine in large excess. In the σ_2 assay, membrane preparations of rat liver served as the source for σ_2 receptors. The nonselective radioligand [^{3}H]DTG was employed in the σ_2 assay because a σ_2-selective radioligand is not yet commercially available. To mask the σ_1 receptors, an excess of non-tritiated (+)-pentazocine was added to the assay solution, while a high concentration of non-tritiated DTG was used to determine nonspecific binding.

Table 3. Affinities of compounds RC-33·HCl toward σ_1, σ_2, NMDA, μ-, κ- and δ-opioid receptors.

Compd[a]	$K_i \pm$SEM [nM][b]		Displacement of specific radioligands [%]			
	σ_1	σ_2	μ	κ	δ	NMDA
RC-33	0.9 ± 0.3	29 ± 5	0	36	0	25
(*S*)-RC-33	1.9 ± 0.2	34 ± 8	12	0	0	11
(*R*)-RC-33	1.8 ± 0.1	45 ± 16	14	0	5	8

[a] Compounds were tested as hydrochlorides. [b] Values are means ± SEM of three experiments.

toward the σ_1 receptor subtype (K_i values < 2 nM, Table 3) and good selectivity over the σ_2, μ-, κ- and δ-opioid receptors, as well as the PCP binding site of NMDA receptors. Concerning the role of chirality in σ_1 receptor binding, the two enantiomers and *rac*-RC-33·HCl are endowed with similar affinities for the σ_1 receptor. Importantly, this observation supports the notion that the interaction of these compounds with this biological target is non-stereoselective.

MD simulations

For a molecular-level explanation of the non-stereoselective binding of RC-33 enantiomers to the σ_1 receptor, the putative binding modes of (*R*)- and (*S*)-RC-33 on our σ_1 receptor 3D homology model were retrieved by exploiting the currently available preliminary information on sequence–structure relationships and mutagenesis studies.[7,11] To summarize briefly, a protein isoform lacking residues 119–149 was found devoid of ligand binding capacity, and the conversion of residues Asp126 and Glu172 into glycine led to a severalfold decrease in ligand binding at the σ_1 receptor.[11c] Moreover, our hydrophobicity analysis[7] and other structure–activity relationship (SAR) studies[11a,b] identified, the transmembrane (TM) regions aside, a third hydrophobic region matching the steroid binding domain like II (SBDLII) region and centered on Asp188, a residue specifically photolabeled with [^{125}I]3-iodo-4-azidococaine ([^{125}I]IACoc).[12] Having localized this protein region as a possible zone for ligand binding, the two enantiomers of RC-33 were then docked into the putative binding site of our 3D receptor model, and their affinity toward the receptor was scored by MM/PBSA analysis.[13]

In a typical structure of the MD-simulated σ_1–ligand complexes, both (*R*)- and (*S*)-RC-33 are oriented horizontally inside the receptor binding pocket and adopt similar binding poses, as illustrated in Figure 3. For both enantiomers, the $-NH^+$ moiety of the ligand piperidine ring is anchored around the negatively charged side chain of Asp126 from the σ_1 protein, interacting with each other through a permanent salt bridge. As tracked by MD simulations, the average distance for the salt bridge through the proton at the cationic moiety of RC-33 and the COO^- group of σ_1 Asp126 is 2.9 ± 0.1 Å for the *R* enantiomer and 2.7 ± 0.1 Å for the *S* enantiomer (Figure 4). The two aromatic rings of RC-33 are packed parallel to Tyr120 and perpendicularly with respect to Tyr173, resulting in strongly stabilizing π–π interactions. Lastly, as can be appreciated from

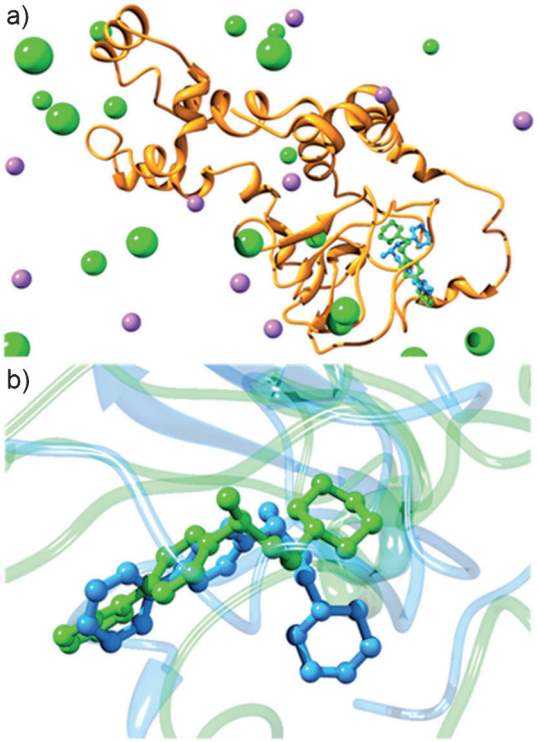

Figure 3. a) Overlay of representative structures for (*R*)-RC-33 (light-blue ball-and-stick model) and (*S*)-RC-33 (light-green ball-and-stick) in complex with the σ_1 receptor (orange ribbon), taken from equilibrated MD snapshots. Some Na^+ and Cl^- ions are also shown as purple and light-green spheres, respectively. Hydrogen atoms and water molecules are omitted for clarity. b) Zoomed-in view of the binding modes of (*R*)- (blue) and (*S*)-RC-33 (green) in the σ_1 binding pocket. In this image, the protein is portrayed in semi-transparent ribbon, colored according to the respective ligand.

Figure 4, in both cases the entire RC-33 molecule is nicely lined by the side chains of several other σ_1 residues, and the relevant hydrophobic interactions which originate from these intermolecular contacts all contribute to stabilize receptor–ligand binding.

The similar binding mode and the equivalent type and number of interactions predicted for (*R*)- and (*S*)-RC-33 in complex with the σ_1 receptor constitute the molecular rationale, according to which our MM/PBSA[13] estimated binding affinities (ΔG_{bind}) for these two enantiomers for the protein are nearly identical, that is, $\Delta G_{bind} = -11.42 \pm 0.29$ kcal mol^{-1} for (*R*)-RC-33 and $\Delta G_{bind} = -11.15 \pm 0.31$ kcal mol^{-1} for (*S*)-RC-33. In accordance with the components of the binding free energy in Figure 5a, for both σ_1–RC-33 enantiomer complexes, van der Waals (ΔE_{VDW}) and electrostatic (ΔE_{ELE}) interactions in the gas phase provide the major favorable contributions to ligand binding. Nonpolar solvation energies (ΔG_{NP}), resulting from the burial of RC-33 solvent-accessible surface area, also afford positive contributions to the binding affinity. Conversely, polar solvation energies (ΔG_{PB}) and entropy components ($-T\Delta S$) oppose binding by making unfavorable contributions to ΔG_{bind}.

To analyze in detail the similarities and differences in the binding modes of the two RC-33 enantiomers with the σ_1 re-

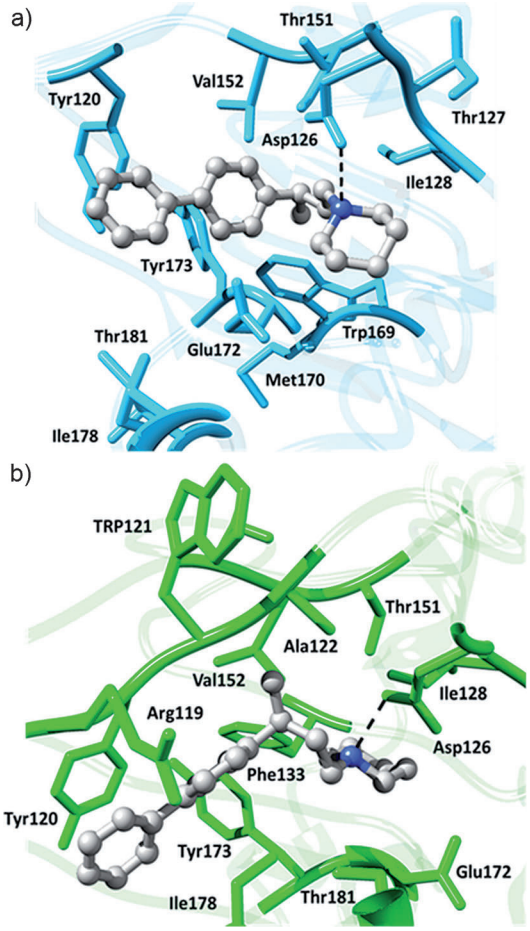

Figure 4. Equilibrated MD snapshots of a) (*R*)-RC-33 and b) (*S*)-RC-33 in complex with the σ_1 receptor; the images are zoomed-in views of the receptor binding site. The protein is depicted in semi-transparent light-blue and light-green ribbon, respectively, while both enantiomers are shown as ball-and-stick models colored according to atom type (C, gray; N, blue; H atoms omitted). Protein residues mainly involved in interaction with the ligands are highlighted as colored sticks and are labeled. Salt bridge interactions are shown as dashed black lines. Water molecules and counterions are omitted for clarity.

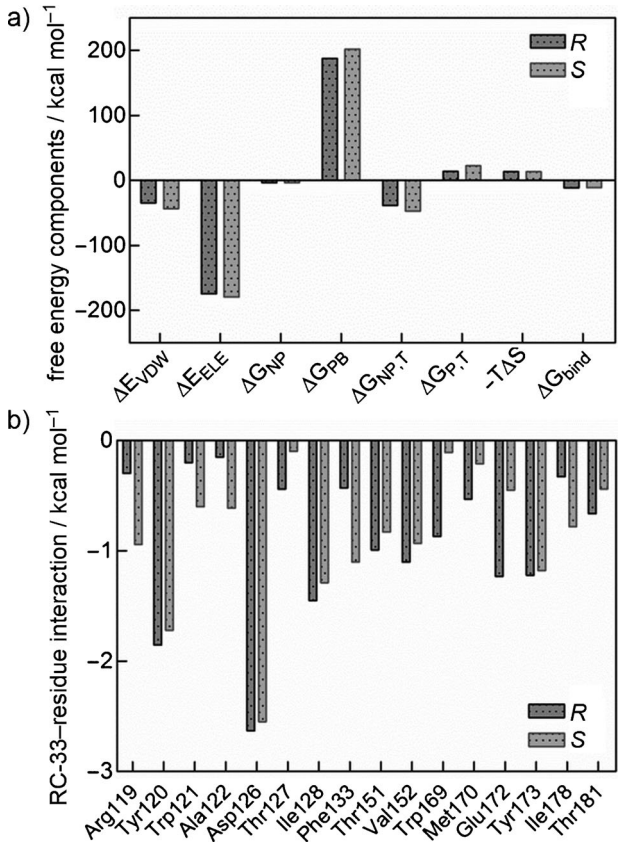

Figure 5. a) Energy components for the binding of (*R*)- and (*S*)-RC-33 to the σ_1 receptor. ΔE_{VDW}, van der Waals energy; ΔE_{ELE}, electrostatic energy; ΔG_{NP}, nonpolar solvation energy; ΔG_{PB}, polar solvation energy; $\Delta G_{NP,T} = \Delta E_{VDW} + \Delta G_{NP}$; $\Delta G_{P,T} = \Delta E_{ELE} + \Delta G_{PB}$; $-T\Delta S$, total entropy contribution; $\Delta G_{bind} = \Delta G_{NP,T} + \Delta G_{P,T} - T\Delta S$. b) Per-residue free-energy contribution to the binding of (*R*)- and (*S*)-RC-33 to the σ_1 receptor.

ceptor, the binding free energy was further decomposed into ligand–residue pairs to create the receptor–residue interaction spectrum shown in Figure 5b. As can be observed, the interaction spectra of the two complexes are similar to each other, with the major contributions stemming from a few groups centered around residues Asp126, Tyr120, and Glu172 in both cases, as expected. Furthermore, for interacting residues that are not shared by the two enantiomers of RC-33 upon binding to the σ_1 receptor (i.e., Thr127, Trp169, and Met170 for the *R* enantiomer, and Arg119, Trp121, and Phe133 in the case of the *S* enantiomer), a sort of compensatory effect is present, ultimately resulting in the non-stereoselective binding of the σ_1 receptor to RC-33.

NGF-induced neurite outgrowth in PC12 cells and cytotoxicity

Pure enantiomers of RC-33·HCl were tested in our validated PC12 cell model of neuronal differentiation to analyze their effect on NGF-induced neurite outgrowth. In previous experiments on PC12 cells *rac*-RC-33·HCl displayed an agonist profile, consistently and significantly potentiating NGF-induced neurite outgrowth at concentrations as low as 0.25 μM.[1c] Therefore, we chose this concentration to test (*S*)- and (*R*)-RC-33·HCl on PC12 cells. *rac*-RC-33·HCl and its enantiomers appear to be almost equally effective. Indeed, both enantiomers were able to increase the percentage of cells with neurite outgrowth with respect to NGF alone (152.8 ± 7.6%, $p < 0.01$ and 143.1 ± 3.8% $p < 0.01$ for (*S*)- and (*R*)-RC-33·HCl, respectively), showing an effect very similar to that of *rac*-RC-33·HCl (157.7 ± 11.0%, $p < 0.001$) (Figure 6). Additionally, their effect was totally blocked by co-administration of the selective σ_1 antagonist NE-100. Taken together, these results confirm that (*S*)- and (*R*)-RC-33·HCl similarly modulate NGF-induced neurite outgrowth, specifically acting as σ_1 receptor agonists.

Finally, an MTT-based cytotoxicity assay, performed after treating HaCaT cells with (*S*)- or (*R*)-RC-33·HCl and with *rac*-RC-

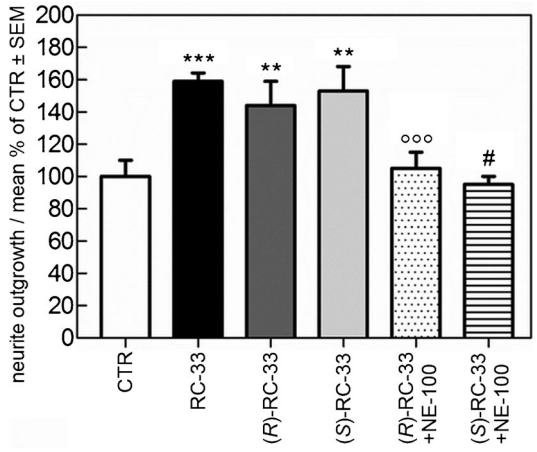

Figure 6. Potentiating effect of σ_1 receptor ligands RC-33·HCl and enantiomers (at 0.25 μM) on neurite outgrowth induced by NGF (2.5 ng mL^{-1}). NE-100 (3 μM) co-administration totally blocked the potentiating effect. Histograms represent the mean ± SEM of at least three different experiments. Data are expressed as percentage of control (CTR; NGF alone). ANOVA: $p < 0.0005$; Tukey's post-hoc test: ***$p < 0.001$; **$p < 0.01$ vs. NGF alone; °°°$p < 0.001$ vs. (−)-(*R*)-RC-33·HCl; #$p < 0.05$ vs. (+)-(*S*)-RC-33·HCl.

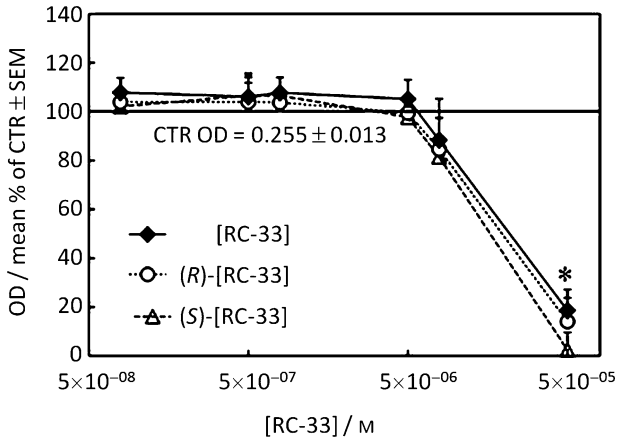

Figure 7. Effect of σ_1 receptor ligands RC-33·HCl and enantiomers on HaCaT cell viability. Values are the mean ± SEM of at least three different experiments. ANOVA: $p < 0.0001$; Tukey's post-hoc test: *$p < 0.0001$ CTR vs. (*R*)-RC-33·HCl, (*S*)-RC-33·HCl, and *rac*-RC-33·HCl.

33·HCl for 48 h (Figure 7) or 72 h (data not shown) confirmed that, similarly to the racemic mixture, both enantiomers are nontoxic at the concentration used in our NGF-induced neurite outgrowth experiments.

In vitro metabolic stability studies

To investigate the role of chirality on metabolic processes, the hepatic metabolic stability of RC-33·HCl enantiomers was tested in vitro using rat and human liver S9 fraction. We previously described *rac*-RC-33·HCl in vitro metabolic stability in several biological matrices, such as mouse and rat blood, rat, dog and human plasma, as well as rat and human liver S9 fractions, containing microsomes (metabolic enzymes of phase I) and cytosol (metabolic enzymes of phase II).[1d] *rac*-RC-33·HCl showed high metabolic stability in all the investigated matrices, with the only exception of liver S9 fractions in the presence of NADPH. Therefore, in the present work we addressed our attention at evaluating the hepatic metabolism of (*R*)- and (*S*)-RC-33·HCl in rat and human liver S9 fractions both in the presence and in the absence of NADPH. To this aim, our previously validated and reproducible method using an ultrafast liquid chromatography system interfaced with a photodiode array detector (UPLC/UV/PAD, Acquity, Waters) was applied.[1d] Briefly, UPLC/UV/PAD analyses were carried out with a BEH Shield RP18 column, eluting with a mixture of water and methanol, containing 0.1% formic acid, in gradient at a flow rate of 0.5 mL min^{-1}. Calibration curves in the range of 1–200 μM (eight points of calibration) were determined, adding known concentrations of each enantiomer of RC-33·HCl to each considered biological matrix, previously deproteinized. In all cases calibration curves with a quadratic correlation coefficient (R^2) of 0.9999 were obtained. Quantification was performed by comparing the chromatographic peak areas for test solutions with those of external standard. The matrices could be directly analyzed by UPLC without clean-up steps.

Similarly to the racemate, both RC-33·HCl enantiomers underwent relatively weak non-oxidative metabolism, with degradation of ~30% within 4 h at 37 °C, both in rat and human (Figure 8). In contrast, they were subjected to a relevant oxidative metabolism in both rat and human liver S9 fractions within the same frame time at 37 °C. Notably, degradation of ~50% in both rat and human was evidenced for (*R*)-RC-33·HCl, while degradation of ~70% in both the biological matrices

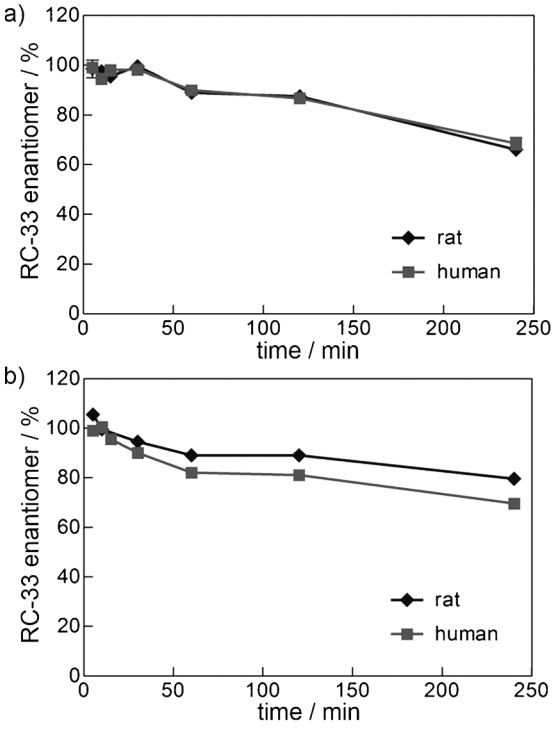

Figure 8. Degradation time courses of a) (*S*)-RC-33·HCl and b) (*R*)-RC-33·HCl in rat and human liver S9 fractions in the absence of NADPH at 37 °C. Data are expressed as the mean ± SD of two independent experiments.

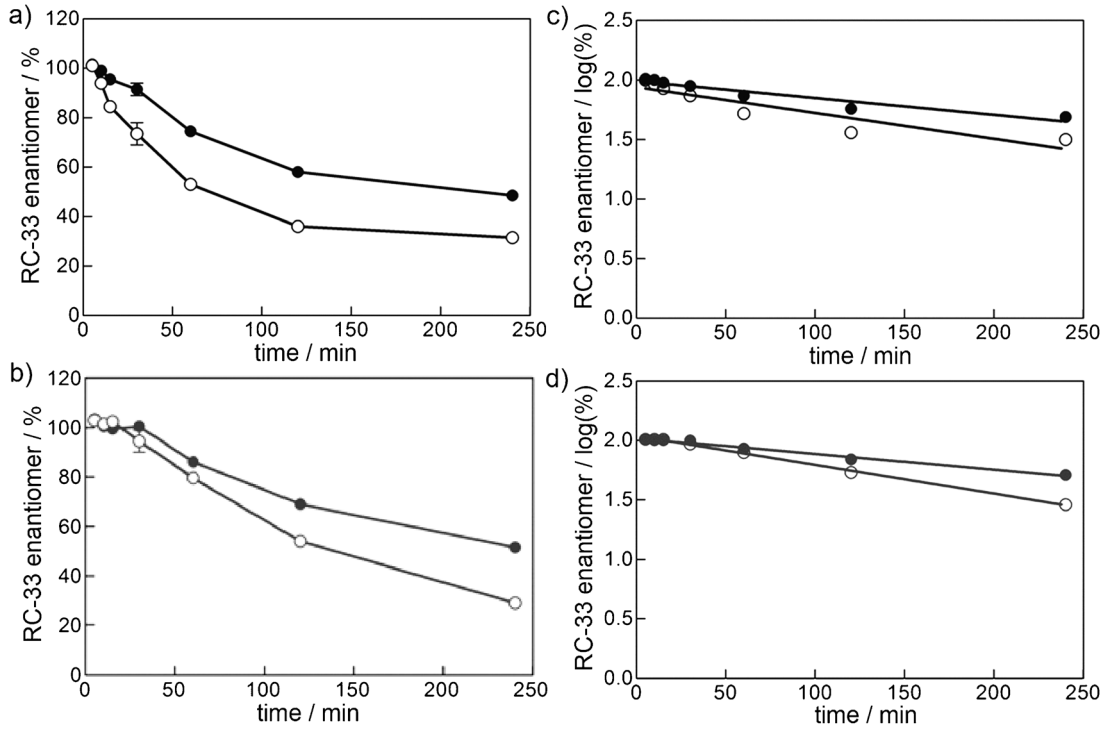

Figure 9. Degradation time courses of (*S*)-RC-33·HCl (○) and (*R*)-RC-33·HCl (●) in a) rat and b) human liver S9 fractions in presence of NADPH at 37 °C. Data are expressed as the mean ± SD of two independent experiments. Enantiomers of RC-33·HCl showed significant degradation in liver S9 fractions in the presence of NADPH, following first-order kinetics, as confirmed by the respective semi-logarithmic plots for c) rat and d) human.

was observed for (*S*)-RC-33·HCl (Figure 9a,b). Moreover, as clearly shown in the semi-logarithmic plots shown in Figure 9c,d, the oxidative degradation of both enantiomers follows first-order kinetics, with a half-life ($t_{1/2}$) of 112 min in rat and 130 min in human for (*S*)-RC-33·HCl, and of 225 min in rat and 246 min in human for (*R*)-RC-33·HCl. Overall, results of the in vitro hepatic metabolic stability studies clearly show that RC-33·HCl enantiomers are similarly metabolized by non-oxidative processes in both rat and human; on the other hand, their degradation in the presence of NADPH was unequivocally proven to be enantioselective with a preference for the *S* enantiomer in both species.

Conclusions

In the present work we addressed the role of chirality in the biological activity of RC-33, recently studied by us in its racemic form. RC-33 enantiomers were isolated by enantioselective semi-preparative HPLC, and their absolute configuration was assigned by applying an integrated CD analysis/chemical correlation strategy. Their in vitro binding affinities toward σ, opioid, and PCP binding site of the NMDA receptors were investigated, and their agonist/antagonist profiles at σ_1 receptor were derived. In synthesis, (*R*)-RC-33 and (*S*)-RC-33 showed nearly the same affinity for the σ_1 receptor and were equally effective as σ_1 receptor agonists, without toxic effects at the concentration shown to be effective. To provide a rational in silico explanation of the experimental evidence that the interaction between RC-33 enantiomers and the σ_1 receptor is non-stereoselective, the two enantiomers were docked into the putative binding site of our 3D receptor model, and their affinity toward the receptor was scored by MM/PBSA analysis. The results of our modeling investigations confirm that both enantiomers of RC-33 can be accommodated within the σ_1 binding site and establish the same network of stabilizing interactions with the target, supporting the non-stereoselective binding of RC-33 to the σ_1 receptor. Lastly, the hepatic metabolic stability of RC-33 enantiomers was also tested in vitro using rat and human liver S9 fractions. (*S*)- and (*R*)-RC-33 were similarly metabolized by non-oxidative processes in both rat and human. Interestingly, compared with the corresponding enantiomer, (*S*)-RC-33·HCl was preferentially metabolized in the presence of NADPH in both rat and human, thus proving that the oxidative metabolic processes possess the same enantiomeric preference in both species.

In summary, based on the overall results of the biological investigations, (*R*)-RC-33 emerged as the eutomer. Because σ_1 receptor agonists such as PRE-084 were recently shown to be promising candidates for a therapeutic strategy for ALS,[14] (*R*)-RC-33 represents the optimal candidate for the in vivo investigation. Its pharmacokinetic profile and results of both short- and long-term investigations as drug candidate in an animal model of ALS will be reported in due course.

Experimental Section

Chemistry

Reagents and instrumentation: Reagents and solvents for synthesis were obtained from Aldrich (Italy). Unless otherwise specified,

commercially available reagents were used as received from the supplier. The catalyst (*R*,*R*)-Ir(ThrePHOX) was purchased from Strem Chemicals, Inc. (Bichheim, France) and stored under nitrogen in a Schlenk flask. Solvents were purified according to the guidelines in *Purification of Laboratory Chemicals*.[15] Microwave dielectric heating was performed in a Discover LabMate instrument (CEM Corporation) specifically designed for organic synthesis and following an appropriate microwave program. Enantioselective hydrogenation reactions were carried out using a Parr multireactor, allowing up to six reactions in parallel under hydrogen pressure. All solvents were evaporated under reduced pressure using a Heidolph Laborota 4000 instrument. Melting points were measured on an SMP3 Stuart Scientific apparatus and are uncorrected. Analytical thin-layer chromatography (TLC) was carried out on silica gel pre-coated glass-backed plates (Fluka Kieselgel 60 F_{254}, Merck) and visualized by UV light, acidic ammonium molybdate(IV), or potassium permanganate. Flash chromatography (FC) was performed with silica gel 60 (particle size 230–400 mesh) purchased from Nova Chimica (Cinisello Balsamo, Italy). IR spectra were recorded on a Jasco (Cremella, LC, Italy) FTIR-4100 spectrophotometer with ATR module; only notable absorptions are given. ^{1}H NMR spectra were recorded on a Bruker Avance 400 spectrometer operating at 400.13 MHz; chemical shifts (δ) are reported in ppm with the solvent reference relative to tetramethylsilane (TMS) employed as the internal standard ($CDCl_3$, $\delta = 7.26$ ppm; CD_2Cl_2, $\delta = 5.32$ ppm; [D_6]acetone, $\delta = 2.05$ ppm). The following abbreviations are used to describe spin multiplicity: s = singlet, d = doublet, t = triplet, q = quartet, m = multiplet, br = broad signal, dd = double-doublet, td = triple-doublet. Coupling constant values are reported in Hz. ^{13}C NMR spectra were recorded on a 400 MHz spectrometer operating at 100.56 MHz, with complete proton decoupling. Carbon chemical shifts (δ) are reported in ppm relative to TMS with the respective solvent resonance as the internal standard ($CDCl_3$, $\delta = 77.23$ ppm; CD_2Cl_2, $\delta = 54.00$ ppm; [D_6]acetone, $\delta = 29.84$ ppm). High-resolution MS spectra were recorded with a Fourier transform ion cyclotron resonance (FT-ICR) instrument equipped with an ESI source. MS analyses were performed on a Finnigan LCQ Fleet system equipped with an ESI source, controlled by Xcalibur software 1.4 (Thermo Finnigan, San Jose, CA, USA). ESI mass spectra were generated in both positive and negative ion modes as necessary. High-performance liquid chromatography (HPLC) runs were conducted on a Jasco (Cremella, LC, Italy) HPLC system equipped with a Jasco AS-2055 plus autosampler, a PU-2089 plus quaternary gradient pump, and an MD-2010 plus multi-wavelength detector. Experimental data were acquired and processed by Jasco Borwin PDA and Borwin Chromatograph Software. Solvents used for chiral chromatography were HPLC grade and supplied by Carlo Erba (Milan, Italy). All HPLC analyses were performed at room temperature. UPLC analyses were performed with a UPLC system (Acquity, Waters) interfaced with a UV detector. Optical rotation values were measured on a Jasco (Cremella, LC, Italy) photoelectric polarimeter DIP 1000 with a 1 dm cell at the sodium D line ($\lambda = 589$ nm); sample concentration values (c) are given in 10^{-2} g mL^{-1}. Circular dichroism (CD) spectra were recorded on a Jasco J-710 instrument.

Chiral chromatography: The enantiomers of RC-33 were completely resolved by a semi-preparative process using a Daicel Chiralcel OJ-H column ($\varnothing = 1$ cm, $l = 25$ cm, 5 μm), eluting with CH_3OH/Et_3N 100:0.1 at RT at a flow rate of 3 mL min^{-1} (Table 1). The eluate was properly partitioned according to the UV profile. Analytical control of collected fractions was performed on a Daicel Chiralcel OJ-H column ($\varnothing = 0.46$ cm, $l = 15$ cm, 5 μm) eluting with CH_3OH/Et_3N 100:0.1 at RT at a flow rate of 0.5 mL min^{-1} and UV detection at $\lambda = 250$ nm. The fractions obtained containing the enantiomers were evaporated at reduced pressure.

(+)-(*S*)-1-(3-(Biphenyl-4-yl)butyl)piperidine [(+)-(*S*)-RC-33]: Yellow oil: 99.5% *ee* determined by analytical chiral HPLC: $t_R = 9.91$ min; $[\alpha]_D^{20} = +22.1$ ($c = 0.3$ in CH_3OH); ^{1}H NMR (400 MHz, CD_2Cl_2): $\delta =$ 7.62 (m, 2H), 7.55 (d, ^3J(H,H) = 8.3 Hz, 2H), 7.44 (t, ^3J(H,H) = 7.7 Hz, 2H), 7.36–7.32 (m, 1H), 7.30 (d, ^3J(H,H) = 8.2 Hz, 2H), 2.82 (m, 1H), 2.32 (m, 4H), 2.26–2.14 (m, 2H), 1.79 (m, 2H), 1.55 (m, 4H), 1.43 (m, 2H), 1.29 ppm (d, ^3J(H,H) = 7.0 Hz, 3H); ^{13}C NMR (100 MHz, CD_2Cl_2): $\delta = 147.6$, 141.6, 139.2, 129.3, 128.0, 127.6, 127.5, 58.0, 55.2, 38.3, 36.1, 26.8, 25.2, 22.8 ppm; IR (ATR): $\tilde{\nu} = 3056$, 3027, 2927, 2850, 2799, 2761, 1598, 1486, 1450, 1153, 1119, 835, 764 cm^{-1}; HRMS-ESI: m/z $[M+H]^+$ calcd for $C_{21}H_{28}N$: 294.2222, found 294.2215. By treatment of (+)-(*S*)-RC-33 with 37% HCl in CH_3OH under stirring (30 min) followed by solvent evaporation, pure (+)-(*S*)-RC-33·HCl was obtained as a white solid: mp: 165–166 °C (dec.); $[\alpha]_D^{20} = +15.8$ ($c = 0.2$ in CH_3OH).

(−)-(*R*)-1-(3-(Biphenyl-4-yl)butyl)piperidine [(−)-(*R*)-RC-33]: Yellow oil: 99.6% *ee* determined by analytical chiral HPLC: $t_R = 11.44$ min; $[\alpha]_D^{20} = -22.2$ ($c = 0.3$ in CH_3OH). Spectroscopic properties comply with those reported for (*S*)-RC-33. HRMS-ESI: m/z $[M+H]^+$ calcd for $C_{21}H_{28}N$: 294.2222, found 294.2218. By treatment of (−)-(*R*)-RC-33 with 37% HCl in CH_3OH under stirring (30 min) followed by solvent evaporation, pure (−)-(*R*)-RC-33·HCl was obtained as a white solid: mp: 165–166 °C (dec.); $[\alpha]_D^{20} = -15.9$ ($c = 0.2$ in CH_3OH).

Typical procedure for the synthesis of (*E*)-1 and (*E*)-2: A solution of ethyl 2-butynoate (2.2 mL, 19 mmol), in 1,2-dichloroethane (DCE, 150 mL) and tetrabutylammonium iodide (21 g, 57 mmol) was heated at reflux for 24 h. The reaction mixture was then cooled, diluted with CH_2Cl_2, washed with $NaHSO_3$ (20% aqueous solution), saturated $NaHCO_3$, and brine. The organic phase, dried over Na_2SO_4 and evaporated, gave crude (*E*)-**3**, that was finally purified by FC, eluting with *n*-hexane, then *n*-hexane/EtOAc 9:1, yielding pure (*E*)-**3** as a colorless oil (4.36 g, 84%), the spectroscopic properties of which comply with reported values.[9a] (*E*)-**3** (2.1 g, 7.6 mmol) was then added to a solution of the appropriate boronic acid (3.7 g for phenyl boronic acid and 6.0 g for biphenyl boronic acid, 30.4 mmol), Cs_2CO_3 (7.4 g, 22.8 mmol), $Pd_2(dba)_3$ (696 mg, 0.76 mmol), P(*t*Bu)$_3$·HBF_4 (882 mg, 3.04 mmol) in freshly distillated THF (92 mL) under nitrogen atmosphere. The reaction mixture was heated at reflux for 4 h, then cooled, diluted with Et_2O, washed with brine, dried over Na_2SO_4, and evaporated to dryness, yielding crude (*E*)-**1** and (*E*)-**2**. Pure products were finally obtained by FC.

(*E*)-Ethyl 3-(biphenyl-4-yl)but-2-enoate [(*E*)-1]: Purification by FC (*n*-hexane, *n*-hexane/Et_2O 99:1, then *n*-hexane/Et_2O 95:5) gave the desired product as a white solid (1.64 g, 81%): mp: 82–84 °C. Spectroscopic properties agree with published data.[16]

(*E*)-Ethyl 3-phenylbut-2-enoate [(*E*)-2]: Purification by FC (*n*-hexane, then *n*-hexane/Et_2O 99:1) gave the desired product as a colorless oil (1.23 g, 85%). Spectroscopic properties comply with those reported previously.[9b]

General procedure for the enantioselective hydrogenation reaction: Catalyst (*R*,*R*)-Ir(ThrePHOX) (49.9 mg, 0.029 mmol) was weighed in a special glass vessel. The vessel was purged with nitrogen, and a 0.362 M CH_2Cl_2 solution (8 mL) of the appropriate substrate (772 mg for (*E*)-**1** and 552 mg for (*E*)-**2**, 2.9 mmol) was added. The vessel was placed into an autoclave and purged three times with hydrogen at 70 bar. The reaction was stirred overnight at RT under pressure of hydrogen; the hydrogen was then released, CH_2Cl_2 was evaporated, and the conversion was determined by NMR analysis

of the crude. The desired products were purified by FC, and enantiomeric excess was determined by chiral HPLC.

(+)-(*S*)-Ethyl 3-(biphenyl-4-yl)butanoate [(+)-(*S*)-4]: Purification by FC (*n*-hexane/EtOAc 97:3) gave the desired product as a yellow oil (739 mg, 95%): 87% *ee* determined by analytical chiral HPLC [Daicel Chiralcel OJ-H (∅ = 0.46 cm, *l* = 15 cm, 5 μm), *n*-heptane/ 2-propanol 90:10, flow rate = 0.8 mL min^{-1}, λ = 250 nm]: $t_{R\,major}$ = 8.69 min, $t_{R\,minor}$ = 11.24 min; $[\alpha]_D^{20} = +29.5$ (*c* = 0.5 in $CHCl_3$); ^{1}H NMR (400 MHz, $CDCl_3$): δ = 7.58 (m, 2H), 7.54 (d, ^3J(H,H) = 8.3 Hz, 2H), 7.43 (t, ^3J(H,H) = 7.6 Hz, 2H), 7.34 (m, 1H), 7.31 (d, ^3J(H,H) = 8.3 Hz, 2H), 4.10 (q, ^3J(H,H) = 7.1 Hz, 2H), 3.34 (m, 1H), 2.66 (dd, AB system, ^2J(H,H) = 15 Hz, ^3J(H,H) = 7.1 Hz, 1H), 2.58 (dd, AB system, ^2J(H,H) = 15 Hz, ^3J(H,H) = 8.1 Hz, 1H), 1.35 (d, ^3J(H,H) = 7.0 Hz, 3H), 1.20 ppm (t, ^3J(H,H) = 7.1 Hz, 3H); ^{13}C NMR (100 MHz, $CDCl_3$): δ = 172.6, 145.1, 141.2, 139.5, 128.9, 127.4, 127.3, 127.2, 60.5, 43.2, 36.4, 22.0, 14.4 ppm; MS (ESI): *m/z*: 269.12 $[M+H]^+$.

(+)-(*S*)-Ethyl 3-phenylbutanoate [(+)-(*S*)-5]: Purification by FC (*n*-hexane/EtOAc 98:2) gave the desired product as colorless oil (546 mg, 98%): 87% *ee* determined by analytical chiral HPLC [Daicel Chiralcel OJ-H (∅ = 0.46 cm, *l* = 15 cm, 5 μm), *n*-heptane/ 2-propanol 90:10, flow rate = 0.8 mL min^{-1}, λ = 250 nm]: $t_{R\,minor}$ = 5.36 min, $t_{R\,major}$ = 5.91 min; $[\alpha]_D^{20} = +18.3$ (*c* = 0.5 in $CHCl_3$). Spectroscopic properties comply with those reported earlier.[10]

(+)-(*S*)-3-(Biphenyl-4-yl)butanoic acid [(+)-(*S*)-6]: To a solution of (+)-(*S*)-**4** (456 mg, 1.7 mmol) in EtOH (23 mL), 2.0 M NaOH (23 mL) was added. The mixture was stirred at RT for 2 h, concentrated under vacuum, adjusted to pH 2 with HCl (1.0 M) and extracted with CH_2Cl_2 (3×40 mL). The combined organic phases were dried over anhydrous Na_2SO_4 and evaporated to dryness, yielding the desired product as a white solid (401 mg, 98%): 87% *ee* determined by analytical chiral HPLC [Daicel Chiralpak IC (∅ = 0.46 cm, *l* = 15 cm, 5 μm), *n*-heptane/2-propanol/TFA 96:4:0.1, flow rate = 0.8 mL min^{-1}, λ = 250 nm]: $t_{R\,major}$ = 8.31 min, $t_{R\,minor}$ = 9.85 min; mp: 110–112 °C; $[\alpha]_D^{20} = +33.6$ (*c* = 1.0 in CH_3OH); ^{1}H NMR (400 MHz, [D_6] acetone): δ = 10.6 (br s, 1H), 7.64 (m, 2H), 7.59 (d, ^3J(H,H) = 8.3 Hz, 2H), 7.44 (t, ^3J(H,H) = 7.6 Hz, 2H), 7.39 (d, ^3J(H,H) = 8.2 Hz, 2H), 7.34 (m, 1H), 3.29 (m, 1H), 2.70–2.58 (m, 2H), 1.33 ppm (d, ^3J(H,H) = 7.0 Hz, 3H); ^{13}C NMR (100 MHz, [D_6] acetone): δ = 173.4, 146.3, 141.7, 139.8, 129.6, 128.2, 128.0, 127.7, 127.6, 42.6, 36.8, 22.4 ppm; MS (ESI): *m/z* 239.11 $[M-H]^-$.

(+)-(*S*)-3-(Biphenyl-4-yl)-1-(piperidin-1-yl)butan-1-one [(+)-(*S*)-7]: In a microwave vial, TBTU (321 mg, 1 mmol) was added to a solution of (+)-(*S*)-**6** (120 mg, 0.5 mmol) in THF (16 mL). The mixture was stirred at RT for 5 min, and then a solution of *N*,*N*-diisopropylethylamine (DIPEA, 0.2 mL, 1 mmol) and piperidine (0.1 mL, 1 mmol) in THF (2 mL) was added. The reaction mixture was irradiated by microwave at 25 W, 80 °C for 20 min, and then the solvent was evaporated under vacuum. The residue was then dissolved with CH_2Cl_2 (30 mL), and the organic phase was washed with 0.5 M HCl (3×15 mL), dried over anhydrous Na_2SO_4, and evaporated, yielding the desired product as a yellow oil (147 mg, 96%): 87% *ee* determined by analytical chiral HPLC (Daicel Chiralcel OJ-H (∅ = 0.46 cm, *l* = 15 cm, 5 μm), *n*-heptane/2-propanol 90:10, flow rate = 0.8 mL min^{-1}, λ = 250 nm): $t_{R\,major}$ = 10.09 min, $t_{R\,minor}$ = 12.03 min; $[\alpha]_D^{20} = +11.6$ (*c* = 0.5 in CH_3OH); ^{1}H NMR (400 MHz, $CDCl_3$): δ = 7.57 (m, 2H), 7.53 (d, ^3J(H,H) = 8.2 Hz, 2H), 7.43 (t, ^3J(H,H) = 7.6 Hz, 2H), 7.35–7.31 (m, 3H), 3.59–3.29 (m, 5H), 2.67 (dd, AB system, ^2J(H,H) = 14.7 Hz, ^3J(H,H) = 6.5 Hz, 1H), 2.56 (dd, AB system, ^2J(H,H) = 14.7 Hz, ^3J(H,H) = 7.9 Hz, 1H), 1.59–1.47 (m, 6H), 1.38 ppm (d, ^3J(H,H) = 7.0 Hz, 3H); ^{13}C NMR (100 MHz, $CDCl_3$): δ = 170.8, 145.5, 141.2, 139.6, 128.9, 127.6, 127.4, 127.3, 127.2, 41.5, 36.9, 26.1, 24.6, 21.8 ppm; IR (neat): MS (ESI): *m/z* 308.22 $[M+H]^+$.

(+)-(*S*)-1-(3-(Biphenyl-4-yl)butyl)piperidine [(+)-(*S*)-RC-33]: A solution of (+)-(*S*)-**7** (61 mg, 0.2 mmol) in anhydrous THF (5 mL) was added dropwise to a stirred suspension of $LiAlH_4$ (23 mg, 0.6 mmol) in anhydrous THF (6 mL). The reaction mixture was stirred at RT for 3 h, cooled to 0 °C, slowly quenched with H_2O, stirred for 15 min at RT and finally filtered on a pad of Celite (washing with EtOAc). The filtrate was evaporated, the residue dissolved in EtOAc (30 mL) and extracted with H_2O (3×20 mL). The organic phase was dried over anhydrous Na_2SO_4 and evaporated, yielding the desired compound as a yellow oil (53 mg, 90%): 87% *ee* determined by analytical chiral HPLC [Daicel Chiralcel OJ-H (∅ = 0.46 cm, *l* = 15 cm, 5 μm), CH_3OH/Et_3N 100:0.1, flow rate = 0.5 mL min^{-1}, λ = 250 nm]: $t_{R\,major}$ = 9.91 min, $t_{R\,minor}$ = 11.44 min; $[\alpha]_D^{20} = +19.2$ (*c* = 1.0 in CH_3OH); MS (ESI): *m/z* 294.25 $[M+H]^+$. Spectroscopic properties comply with those reported above for (+)-(*S*)-RC-33 obtained by semi-preparative HPLC.

Circular dichroism: Solutions of (+)-**4** ($c = 6.25\times10^{-5}$ M in *n*-hexane, optical pathway 1 cm) and of (+)-(*S*)-**5** ($c = 2.5\times10^{-5}$ M in *n*-hexane, optical pathway 1 cm) were analyzed in a nitrogen atmosphere. CD spectra were scanned at 10 nm min^{-1} with a spectral band width of 2 nm and data resolution of 0.2 nm. Experimental data are reported in the Supporting Information.

Biological investigations

In vitro binding assays

Materials: Guinea pig brains, rat liver, and rat brains for the σ_1, σ_2, μ-, κ-, and δ-opioid receptor binding assays were commercially available (Harlan–Winkelmann, Borchen, Germany). Pig brains for binding assays to the PCP binding site of the NMDA receptor were a kind donation from a local slaughterhouse (Coesfeld, Germany). Homogenizer: Elvehjem Potter (B. Braun Biotech International, Melsungen, Germany) and Soniprep 150, MSE, London, UK). Centrifuges: Cooling centrifuge model Rotina 35R (Hettich, Tuttlingen, Germany) and High-speed cooling centrifuge model Sorvall RC-5C plus (Thermo Fisher Scientific, Langenselbold, Germany). Multiplates: standard 96-well multiplates (Diagonal, Muenster, Germany). Shaker: self-made device with adjustable temperature and tumbling speed (scientific workshop of the institute). Vortexer: Vortex Genie 2 (Thermo Fisher Scientific, Langenselbold, Germany). Harvester: MicroBeta FilterMate-96 Harvester. Filter: Printed Filtermat Type A and B. Scintillator: Meltilex (Type A or B) solid-state scintillator. Scintillation analyzer: MicroBeta Trilux (all PerkinElmer LAS, Rodgau-Jügesheim, Germany). Chemicals and reagents were purchased from various commercial sources and were of analytical grade.

Preparation of membrane homogenates from guinea pig brain: Five guinea pig brains were homogenized with the potter (500–800 rpm, 10 up-and-down strokes) in six volumes of cold 0.32 M sucrose. The suspension was centrifuged at 1200 *g* for 10 min at 4 °C. The supernatant was separated and centrifuged at 23500 *g* for 20 min at 4 °C. The pellet was resuspended in 5–6 volumes of buffer (50 mM Tris, pH 7.4) and centrifuged again at 23500 *g* (20 min, 4 °C). This procedure was repeated twice. The final pellet was resuspended in 5–6 volumes of buffer and frozen (−80 °C) in 1.5 mL portions containing ~1.5 (mg protein) mL^{-1}.

Preparation of membrane homogenates from rat liver: Two rat livers (Sprague–Dawley rats) were cut into small pieces and homogen-

ized with the potter (500–800 rpm, 10 up-and-down strokes) in six volumes of cold 0.32 M sucrose. The suspension was centrifuged at 1200 *g* for 10 min at 4 °C. The supernatant was separated and centrifuged at 31 000 *g* for 20 min at 4 °C. The pellet was resuspended in 5–6 volumes of buffer (50 mM Tris, pH 8.0) and incubated at RT for 30 min. After incubation, the suspension was centrifuged again at 31 000 *g* for 20 min at 4 °C. The final pellet was resuspended in 5–6 volumes of buffer and stored at −80 °C in 1.5 mL portions containing ~2 (mg protein) mL^{-1}.

Preparation of membrane homogenates from rat brain: Five rat brains (Sprague–Dawley rats) were homogenized with the potter (500–800 rpm, 10 up-and-down strokes) in six volumes of cold 0.32 M sucrose. The suspension was centrifuged at 1200 *g* for 10 min at 4 °C. The supernatant was separated and centrifuged at 23 500 *g* for 20 min at 4 °C. The pellet was resuspended in 5–6 volumes of buffer (50 mM Tris, pH 7.4) and centrifuged again at 23 500 *g* (20 min, 4 °C). This procedure was repeated twice. The final pellet was resuspended in 5–6 volumes of buffer and stored at −80 °C in 1.5 mL portions containing ~1.5 (mg protein) mL^{-1}.

Preparation of membrane homogenates from pig brain cortex: Fresh pig brain cortex was homogenized with the potter (500–800 rpm, 10 up-and-down strokes) in six volumes of cold 0.32 M sucrose. The suspension was centrifuged at 1200 *g* for 10 min at 4 °C. The supernatant was separated and centrifuged at 31 000 *g* for 20 min at 4 °C. The pellet was resuspended in 5–6 volumes of Tris/EDTA buffer (5 mM/1 mM, pH 7.5) and centrifuged again at 31 000 *g* (20 min, 4 °C). The final pellet was resuspended in 5–6 volumes of buffer and frozen (−80 °C) in 1.5 mL portions containing ~0.8 (mg protein) mL^{-1}.

Protein determination: The protein concentration was determined by the method of Bradford[17] modified by Stoscheck.[18] The Bradford solution was prepared by dissolving 5 mg of Coomassie Brilliant Blue G 250 in 2.5 mL EtOH (95% *v/v*). Deionized H_2O (10 mL) and phosphoric acid (85% *w/v*, 5 mL) were added to this solution, and the mixture was stirred and filled to a total volume of 50 mL with deionized water. Calibration was carried out using bovine serum albumin as a standard in nine concentrations (0.1, 0.2, 0.4, 0.6, 0.8, 1.0, 1.5, 2.0, and 4.0 mg mL^{-1}). In a 96-well standard multiplate, 10 μL of the calibration solution or 10 μL of the membrane receptor preparation were mixed with 190 μL of the Bradford solution. After 5 min, the UV absorption of the protein–dye complex at $\lambda = 595$ nm was measured with a plate reader (Tecan Genios, Tecan, Crailsheim, Germany).

General protocol for binding assays: The test compound solutions were prepared by dissolving ~10 μmol (usually 2–4 mg) of test compound in DMSO so that a 10 mM stock solution was obtained. To obtain the required test solutions for the assay, the DMSO stock solution was diluted with the respective assay buffer. The filtermats were presoaked in 0.5% aqueous polyethylenimine solution for 2 h at RT before use. All binding experiments were carried out in duplicate in 96-well multiplates. The concentrations given are the final concentrations in the assay. Generally, the assays were performed by addition of 50 μL of the respective assay buffer, 50 μL test compound solution at various concentrations (10^{-5}, 10^{-6}, 10^{-7}, 10^{-8}, 10^{-9} and 10^{-10} M), 50 μL of corresponding radioligand solution, and 50 μL of the respective receptor preparation into each well of the multiplate (total volume 200 μL). The receptor preparation was always added last. During the incubation, the multiplates were shaken at a speed of 500–600 rpm at the specified temperature. Unless otherwise noted, the assays were terminated after 120 min by rapid filtration using the harvester. During the filtration each well was washed five times with 300 μL of water. Subsequently, the filtermats were dried at 95 °C. The solid scintillator was melted on the dried filtermats at 95 °C for 5 min. After solidifying of the scintillator at RT, the trapped radioactivity in the filtermats was measured with the scintillation analyzer. Each position on the filtermat corresponding to one well of the multiplate was measured for 5 min with the [^{3}H]-counting protocol. The overall counting efficiency was 20%. The IC_{50} values were calculated with GraphPad Prism 3.0 (GraphPad Software, San Diego, CA, USA) by nonlinear regression analysis. The IC_{50} values were subsequently transformed into K_i values using the equation of Cheng and Prusoff.[19] The K_i values are given as mean value ± SEM from three independent experiments.

σ_1 receptor binding assay: The assay was performed with the radioligand [^{3}H](+)-pentazocine (22.0 Ci $mmol^{-1}$; PerkinElmer). The thawed membrane preparation of guinea pig brain cortex (~100 μg protein) was incubated with various concentrations of test compounds, 2 nM [^{3}H](+)-pentazocine, and Tris buffer (50 mM, pH 7.4) at 37 °C. The nonspecific binding was determined with 10 μM unlabeled (+)-pentazocine. The K_d value of (+)-pentazocine is 2.9 nM.

σ_2 receptor binding assay: The assays were performed with the radioligand [^{3}H]DTG (specific activity 50 Ci $mmol^{-1}$; ARC, St. Louis, MO, USA). The thawed membrane preparation of rat liver (~100 μg protein) was incubated with various concentrations of the test compound, 3 nM [^{3}H]DTG, and buffer containing (+)-pentazocine (500 nM (+)-pentazocine in 50 mM Tris, pH 8.0) at RT. The nonspecific binding was determined with 10 μM unlabeled DTG. The K_d value of [^{3}H]DTG is 17.9 nM.

κ opioid receptor binding assay: The assay was performed with the radioligand [^{3}H]U-69,593 (55 Ci $mmol^{-1}$, Amersham, Little Chalfont, UK). The thawed guinea pig brain membrane preparation (~100 μg protein) was incubated with various concentrations of test compounds, 1 nM [^{3}H]U-69,593, and Tris/$MgCl_2$ buffer (50 mM, 8 mM $MgCl_2$, pH 7.4) at 37 °C. The nonspecific binding was determined with 10 μM unlabeled U-69,593. The K_d value of U-69,593 is 0.69 nM.

μ opioid receptor binding assay: The assay was performed with the radioligand [^{3}H]DAMGO (51 Ci $mmol^{-1}$, PerkinElmer). The thawed guinea pig brain membrane preparation (~100 μg protein) was incubated with various concentrations of test compounds, 3 nM [^{3}H]DAMGO, and Tris/$MgCl_2$ buffer (50 mM, 8 mM $MgCl_2$, pH 7.4) at 37 °C. The nonspecific binding was determined with 10 μM unlabeled Naloxon. The K_d value of DAMGO is 0.57 nM.

δ opioid receptor binding assay: The assay was performed with the radioligand [^{3}H]DPDPE (69 Ci $mmol^{-1}$, Amersham). The thawed rat membrane preparation (~75 μg protein) was incubated with various concentrations of test compounds, 3 nM [^{3}H]DPDPE, and Tris/$MgCl_2$/PMSF buffer (50 mM, 8 mM $MgCl_2$, 400 μM PMSF, pH 7.4) at 37 °C. The nonspecific binding was determined with 10 μM unlabeled morphine. The K_d value of DPDPE is 0.65 nM.

PCP binding site of the NMDA receptor binding assay: The assay was performed with the radioligand [^{3}H](+)-MK-801 (22.0 Ci $mmol^{-1}$; PerkinElmer). The thawed membrane preparation of pig brain cortex (~100 μg protein) was incubated with various concentrations of test compounds, 2 nM [^{3}H](+)-MK-801, and Tris/EDTA buffer (5 mM/1 mM, pH 7.5) at RT. The nonspecific binding was determined with 10 μM unlabeled (+)-MK-801. The K_d value of (+)-MK-801 is 1.26 nM.

Molecular simulations

The model structures of (*R*)- and (*S*)-RC-33 were sketched and geometrically optimized using Discovery Studio (DS, version 2.5, Accelrys, San Diego, CA, USA). A conformational search was then carried out using a well-validated, ad hoc developed combined molecular mechanics/molecular dynamics simulated annealing (MDSA) protocol[7,11a,b,20] using Amber 11.[21] Accordingly, the relaxed structures were subjected to five repeated temperature cycles (from 300 to 1000 K and back) using constant-volume/constant-temperature (NVT) MD conditions. At the end of each annealing cycle, the structures were again energy minimized to converge below 10^{-4} kcal mol^{-1} Å, and only the structures corresponding to the minimum energy were used for further modeling. The atomic partial charges for the geometrically optimized compounds were obtained using the RESP procedure,[22] and the electrostatic potentials were produced by single-point quantum mechanical calculations at the Hartree–Fock level with a 6-31G* basis set, using the Merz–Singh–Kollman van der Waals parameters.[23] Eventual ff03[24] missing force field parameters for the RC-33 enantiomers were generated using the general Amber force field (GAFF)[25] of Amber 11. The optimized structures of (*R*)- and (*S*)-RC-33 were then docked into the σ_1 putative binding pockets by applying a consolidated procedure;[7,11a,b,26] accordingly, it is described herein only briefly. All docking experiments were performed with AutoDock 4.3/AutoDock Tools 1.4.6[27] on a win64 platform. DS was employed to define the size of the binding site, using an opening site of 10 Å and a grid size of 0.7 Å. The dimensions of the AutoDock grid box, based on the cavity identified by DS, was large enough to cover all possible rotations of each ligand. van der Waals interactions and hydrogen bonding (O–H, N–H, and S–H) were modeled with the Amber 12-6 and 12-10 Lennard–Jones parameters, respectively, while the distance-dependent relative permittivity of Mehler and Solmajer[28] was applied in the generation of the electrostatic grid maps. A total of 300 Monte Carlo/simulated annealing (MC/SA) runs were performed, with 100 constant-temperature cycles for simulated annealing. The GB/SA implicit water model[29] was used in these calculations to mimic the solvated environment. The angles of the side chains and the rotation of the angles ϕ and ψ were set free during the calculations, while all other parameters of the MC/SA algorithm were kept as default. The structures of the two compounds were subjected to cluster analysis with a 1 Å tolerance for an all-atom root-mean-square (RMS) deviation from a lower-energy structure representing each cluster family. The resulting docked conformations were clustered and visualized; then, for each compound, only the molecular conformation satisfying the combined criteria of having the lowest (i.e., more favorable) AutoDock energy and belonging to a highly populated cluster was selected to carry for further modeling. Both ligand–receptor complex obtained from the docking procedure was further refined in Amber 11 using the quenched molecular dynamics (QMD) method.[7,11a,b,20,26] According to QMD, 1 ns MD simulations at 300 K were employed to sample the conformational space of each ligand–receptor complex in the GB/SA continuum solvation environment.[29] The integration step was equal to 1 fs. After each picosecond, each system was cooled to 0 K, and the structure was extensively minimized and stored. To prevent global conformational changes of the protein, the backbone atoms of the protein binding site were constrained by a harmonic force constant of 100 kcal Å^{-1}, whereas the amino acid side chains and ligands were allowed to move without constraint. The best energy configuration of each complex resulting from the previous step was subsequently solvated by a cubic box of TIP3P[30] water molecules extending at least 10 Å in each direction from the solute. The system was then neutralized with the addition of 21 Na^+ and 15 Cl^- counterions; furthermore, the solution ionic strength was adjusted to the physiological value of 0.15 M by adding the required amounts of Na^+ and Cl^- ions. Each solvated system was relaxed by 500 steps of steepest descent followed by 500 other conjugate-gradient minimization steps and then gradually heated to a temperature of 300 K in intervals of 50 ps of NVT MD, using a Verlet integration time step of 1.0 fs. The Langevin thermostat was used to control temperature, with a collision frequency of 2.0 ps^{-1}. The SHAKE method[31] was used to constrain all of the covalently bound hydrogen atoms, while long-range nonbonded van der Waals interactions were truncated by using dual cutoffs of 6 and 12 Å. The particle mesh Ewald (PME) method[32] was applied to treat long-range electrostatic interactions. The protein was restrained with a force constant of 2.0 kcal mol^{-1} Å^{-1}, and all simulations were carried out with periodic boundary conditions. The density of each system was subsequently equilibrated via MD runs in the isothermal–isobaric (NPT) ensemble, with isotropic position scaling and a pressure relaxation time of 1.0 ps, for 50 ps with a time step of 1 fs. All restraints on the protein atoms were then removed, and each system was further equilibrated using NPT MD runs at 300 K, with a pressure relaxation time of 2.0 ps. Three equilibration steps were performed, each 2 ns long and with a time step of 2.0 fs. To check the system stability, the fluctuations of the RMSD of the simulated position of the backbone atoms of the σ_1 receptor with respect to those of the initial protein were monitored. All physicochemical parameters and RMSD values showed very low fluctuations at the end of the equilibration process, indicating that the systems reached a true equilibrium condition. Each equilibration phase was followed by a data production run consisting of 4 ns of MD simulations in the canonical (NVT) ensemble. Only the last 2 ns of each equilibrated MD trajectory were considered for statistical data collections. A total of 100 trajectory snapshots were analyzed for each ligand–receptor complex. The binding free energy, ΔG_{bind}, between each ligand and the σ_1 receptor was estimated by resorting to the MM/PBSA approach.[13] According to this well-validated methodology,[7,11a,b,20,26,33] the free energy was calculated for each molecular species (complex, receptor, and ligand), and the binding free energy was computed as the difference:

$$\Delta G_{bind} = G_{complex} - (G_{receptor} + G_{ligand}) = \Delta E_{MM} + \Delta G_{sol} - T\Delta S \quad (1)$$

The molecular mechanics energy ΔE_{MM} was calculated as the sum of the van der Waals and electrostatic interactions:

$$\Delta E_{MM} = \Delta E_{VDW} + \Delta E_{ELE} \quad (2)$$

The solvation free energy term ΔG_{sol} was composed of the polar and nonpolar contributions:

$$\Delta G_{sol} = \Delta G_{PB} + \Delta G_{NP} \quad (3)$$

ΔG_{PB} was estimated using DelPhi,[34] which solves the Poisson–Boltzmann equations numerically and calculates the electrostatic energy according to the electrostatic potential. Dielectric constants of 1 and 80 were used for solute and solvent, respectively. A grid spacing of 0.5 per Å, extending 20% beyond the dimensions of the solute, was employed in these calculations. The nonpolar solvation contribution was determined using the following relationship:[35]

$$\Delta G_{NP} = \gamma \times SA + \beta \quad (4)$$

in which $\gamma = 0.00542$ kcal mol^{-1} Å^{-2}, $\beta = 0.92$ kcal mol^{-1}, and *SA* is the molecular surface area estimated by means of the MSMS software.[36] The conformational entropy (translation, rotation, and vibration) upon ligand binding [$-T\Delta S$ in Eq. (1)] was estimated using normal-mode analysis with the Nmode module of Amber 11.[37] Prior to normal-mode calculations, each MD snapshot of each receptor–ligand complex was energy minimized using a distance-dependent dielectric constant $\varepsilon = 4r_{ij}$ until the RMS of the elements of the gradient vector was $< 10^{-4}$ kcal mol^{-1} Å. To minimize the effects due to different conformations adopted by individual snapshots, and due to the high computational demand of this approach, we averaged the estimation of entropy over MD 40 snapshots for each molecular complex that were evenly extracted from the last 2 ns of each corresponding MD trajectory. The per-residue binding free energy decomposition was performed exploiting the MD trajectory of each given compound–receptor complex, with the aim of identifying the key residues involved in the ligand–receptor interaction. This analysis was carried out using the MM/GBSA approach, and was based on the same snapshots used in the binding free energy calculation. All simulations were carried out using the Sander and Pmemd modules of Amber 11, running in parallel on 256 processors of the PLX calculation cluster of the CINECA supercomputer facility (Bologna, Italy). The entire MD simulation and data analysis procedure was optimized by integrating Amber 11 in modeFRONTIER, a multidisciplinary and multiobjective optimization and design environment.[38]

NGF neurite outgrowth in PC12 cells and cytotoxicity

Cell culture: PC12 cells were cultured at 37 °C, under 5% CO_2 in RPMI 1640 medium supplemented with 5% heat-inactivated fetal bovine serum (FBS), 10% heat-inactivated horse serum (HS), 1% Glutamax, 1% Zell (Biochrom). The medium was changed two or three times a week. When NGF with or without the test compounds had to be added cells were detached from the culture dishes, centrifuged at 150 *g* for 5 min and plated at 8000 cells mL^{-1} onto glass coverslips coated with poly-D-lysine in 12-well tissue culture plates; 24 h after plating, the medium was replaced with RPMI 1640 medium containing 0.5% HS, 1% Glutamax, 1% Zell and with NGF (2.5 ng mL^{-1}) with or without drugs. Stock solutions (10 mM) of compounds RC-33·HCl, (*S*)-RC-33·HCl, and (*R*)-RC-33·HCl were dissolved with apyrogenic H_2O to 1 mM solution and added to the cell medium to reach the selected final concentrations (0.25 μM). In some experiments, the well-characterized σ_1 receptor antagonist NE-100 (10 mM stock solution in apyrogenic H_2O) was co-administered with RC-33·HCl, (*S*)-RC-33·HCl, or (*R*)-RC-33·HCl at a final concentration of 3 μM.

Quantification of neurite outgrowth: Five days after incubation with NGF (2.5 ng mL^{-1}) with or without drugs, PC12 cells, grown on glass coverslips, were fixed at RT for 15 min in phosphate-buffered saline (PBS) containing 4% (*w/v*) paraformaldehyde. Morphometric analysis was performed on digitized images of fixed cells taken under phase-contrast illumination with an inverted microscope (Optika) linked to a digital camera. Images of at least six fields per coverslip were taken at 20× magnification in order to count an average of 300 cells. At least three independent experiments were performed for each condition. Neurite outgrowth was scored by measuring the percentage of differentiated cells bearing at least one neurite longer than the cell body diameter. Cell counting and neurite length measurements were performed in a blind manner by two independent observers using NeuronJ plugin[39] of ImageJ public domain software.

Cytotoxicity test: In vitro spontaneously transformed keratinocytes from histologically normal human skin (HaCaT) were purchased from CLS (Cell Lines Service, D69214 Eppelhein, Germany) and grown in DMEM/high glucose; 2 mM glutamine; Pen/Strep 1%; FBS 10%. Cells were dissociated using an appropriate volume of pre-warmed TrypLE Select cell dissociation reagent (Sigma–Aldrich) to the flask (i.e., 1 mL in a T25 cm^2 flask). Complete growth medium was then added, and the cells were pelletted at 250 *g* for 5 min. HaCaT cells were resuspended in medium with 10% FBS and plated 5000 cells per well in 96-well plates. After 24 h, cells were treated with *rac*-RC-33·HCl, (*R*)-RC-33, or (*S*)-RC-33·HCl in the concentration range of 1×10^{-8} to 1×10^{-5} M and incubated for 48 or 72 h at 37 °C under 5% CO_2 in media with 5% FBS (compounds were tested in triplicate, in $n = 4$ independent experiments). An MTT-based cytotoxicity test (CellTiter 96 AQueous One Solution Cell Proliferation Assay, Promega) was performed, and the optical density was read in a microplate reader (BioTek Instruments, Inc.).

Statistical analysis: Data are expressed as the mean ± standard error of the mean (SEM). Statistical analysis was performed by two-way analysis of variance (ANOVA) and post hoc Tukey's test. Values of $p < 0.05$ were considered statistically significant.

In vitro metabolic study

General procedure: Metabolic stability studies were conducted on liver S9 fraction from rat and human. To make a comparison between oxidative and non-oxidative metabolism of the compound, two studies were performed in parallel, with and without the addition of NADPH cofactor. Briefly, 200 μL of 20 mg mL^{-1} commercial liver S9 were firstly diluted to 0.5 mg mL^{-1} with 0.1 M PBS at pH 7.4; 980 μL of the diluted S9 were then placed in Eppendorf vials in a thermomixer at 37 °C and gentle shaking was applied (300 rpm). NADPH (10 μL, 50 mM in water) was added to the S9 to obtain a test solution with NADPH, while water alone (10 μL) was added to the S9 to obtain an NADPH-independent test solution. Finally, (−)-(*R*)-RC-33·HCl or (+)-(*S*)-RC-33·HCl (10 μL of a 1 mM solution in DMSO) were added to the test solutions and the kinetics measurements started. Aliquots (50 μL) from the reaction mixtures were sampled in duplicate at 5, 10, 15, 30, 60, 120, and 240 min to determine reaction kinetics. The reaction was quenched by adding acetonitrile (150 μL) and DMSO (10 μL) to precipitate the proteins. Samples were vortex mixed and centrifuged at 4000 rpm for 10 min at 4 °C. The supernatant was directly analyzed by UPLC/UV/PAD without clean-up steps to estimate the concentration of test compound at each time point. The extrapolated concentration is useful to calculate the half-life ($t_{1/2}$) of enantiomeric RC-33·HCl in each matrix.

Analytical method: UPLC analyses were carried out on a BEH Shield RP18, 2.1×50 mm, 1.7 mm chromatographic column with gradient mode, using mixtures of mobile phase A [H_2O containing 0.1% formic acid] and mobile phase B [CH_3OH containing 0.1% formic acid], at a flow rate of 0.5 mL min^{-1}. Each analysis lasted 1.7 min with the following gradient: linear decrease from 90 to 0% mobile phase A from 0 to 1 min; 100% of mobile phase B was maintained for 0.5 min before a quick ramp (in 0.1 min) to 90% mobile phase A. The analysis was continued under initial condition for another 0.1 min in isocratic mode. The injection volume for each sample was 5 μL and chromatograms were recorded at $\lambda = 254$ nm. The raw data (average peak area at each time point) were interpolated using Quanlynx v 4.1 software to extrapolate the concentration of test compound at each time point.

Quantification of RC-33 enantiomers: Quantification was performed by comparing the chromatographic peak areas for test solutions with those of an external standard. Calibration curves were obtained by analyzing solutions of RC-33 enantiomers at a known concentration in the range of 1–200 μM in a deproteinized biological matrix, with a matrix/solvent ratio of 1:3. In detail, standard solutions of each enantiomer in DMSO were firstly prepared by serial dilution of 10 mM stock solution to the final concentrations of 1000, 500, 250, 100, 50, 25, 10, and 5 μM; 3 mL of each biological matrix were then precipitated with 9 mL acetonitrile, vortex mixed and centrifuged at 4 °C and 4000 rpm for 10 min; 200 μL of each deproteinized matrix were finally spiked with 10 μL of each standard solution, furnishing solutions with the final nominal concentrations of 200, 100, 50, 20, 10, 5, 2, and 1 μM, which were analyzed in triplicate to create calibration curves.

Abbreviations

[^{3}H]DAMGO: [^{3}H][D-Ala^2,Me-Phe^4,Gly-ol^5]enkephalin; DCE: 1,2-dichloroethane; [^{3}H]DPDPE: [^{3}H](1*S*,6*S*,12*S*)-6-[[(2*S*)-2-amino-3-[4-hydroxyphenyl]propanoyl]amino]-2,2,5,5-tetramethyl-7,10,13-trioxo-12-(phenylmethyl)-3,4-dithia-8,11,14-triazacyclotetradecane-1-carboxylic acid; DTG: [^{3}H]di-*o*-tolylguanidine; [^{3}H]MK-801: [^{3}H](5*R*,10*S*)-(+)-5-methyl-10,11-dihydro-5*H*-dibenzo[α,β]cyclohepten-5,10-imine; MTT: 3-(4,5-dimethylthiazol-2-yl)-2,5-diphenyltetrazolium bromide; NE-100: 4-methoxy-3-(2-phenylethoxy)-*N*,*N*-dipropylbenzeneethanamine hydrochloride; PRE-084: 2-(4-morpholinethyl)1-phenylcyclohexanecarboxylate hydrochloride; TBTU: *O*-(benzotriazol-1-yl)-*N*,*N*,*N*′,*N*′-tetramethyluronium tetrafluoroborate; [^{3}H]U-69,593: [^{3}H](5*R*,7*R*,8β-(−)-*N*-methyl-*N*-[7-(1-pyrrolidinyl)-1-oxaspiro-(4-5)dec-8-yl]benzeneacetamide).

Acknowledgements

D.R., S.C., M.P., and D.C. gratefully acknowledge financial support from ARISLA (Grant SaNet-ALS). E.L., V.D.C., M.F., and S.P. gratefully acknowledge financial support from ESTECO s.r.l. (Grant DDOS). Access to CINECA supercomputing facility was granted through the sponsored Italian Super Computing Resource Allocation (ISCRA), project MONALISA (to S.P.).

Keywords: biological activity · enantioselectivity · in vitro metabolism · neuroprotective agents · σ_1 agonists.

[1] a) S. Collina, G. Loddo, M. Urbano, L. Linati, A. Callegari, F. Ortuso, S. Alcaro, C. Laggner, T. Langer, O. Prezzavento, G. Ronsisvalle, O. Azzolina, *Bioorg. Med. Chem.* **2007**, *15*, 771 – 783; b) D. Rossi, M. Urbano, A. Pedrali, M. Serra, D. Zampieri, M. G. Mamolo, C. Laggner, C. Zanette, C. Florio, D. Schepmann, B. Wuensch, O. Azzolina, S. Collina, *Bioorg. Med. Chem.* **2010**, *18*, 1204 – 1212; c) D. Rossi, A. Pedrali, M. Urbano, R. Gaggeri, M. Serra, L. Fernàndez, M. Fernàndez, J. Caballero, S. Ronsisvalle, O. Prezzavento, D. Schepmann, B. Wuensch, M. Peviani, D. Curti, O. Azzolina, S. Collina, *Bioorg. Med. Chem.* **2011**, *19*, 6210 – 6224; d) D. Rossi, A. Marra, P. Picconi, M. Serra, L. Catenacci, M. Sorrenti, E. Laurini, M. Fermeglia, S. Pricl, S. Brambilla, N. Almirante, M. Peviani, D. Curti, S. Collina, *Bioorg. Med. Chem.* **2013**, *21*, 2577 – 2586.

[2] a) T. Maurice, T. P. Su, *Pharmacol. Ther.* **2009**, *124*, 195 – 206; b) K. W. Crawford, W. D. Bowen, *Cancer Res.* **2002**, *62*, 313 – 322.

[3] A. A. Luty, J. B. J. Kwok, C. Dobson-Stone, C. T. Loy, K. G. Coupland, H. Karlstrom, T. Sobow, J. Tchorzewska, A. Maruszak, M. Barcikowska, P. K. Panegyres, C. Zekanowski, W. S. Brooks, K. L. Williams, I. P. Blair, K. A. Mather, P. S. Sachdev, G. M. Halliday, P. R. Schofield, *Ann. Neurol.* **2010**, *68*, 639 – 649.

[4] A. Al-Saif, F. Al-Mohanna, S. Bohlega, *Ann. Neurol.* **2011**, *70*, 913 – 919.

[5] a) P. Sassone-Corsi, C. J. Der, I. M. Verma, *Mol. Cell. Biol.* **1989**, *9*, 3174 – 3183; b) M. Takebayashi, T. Hayashi, T. P. Su, *J. Pharmacol. Exp. Ther.* **2002**, *303*, 1227 – 1237; c) M. Takebayashi, T. Hayashi, T. P. Su, *Synapse* **2004**, *53*, 90 – 103; d) M. S. Guzmán-Lenis, X. Navarro, C. Casas, *Neuroscience* **2009**, *162*, 31 – 38.

[6] a) I. Agranat, H. Caner, J. Cadwell, *Nat. Rev. Drug Discovery* **2002**, *1*, 753 – 768; b) T. Andersson, *Clin. Pharmacokinet.* **2004**, *43*, 279 – 285.

[7] E. Laurini, V. Dal Col, M. G. Mamolo, D. Zampieri, P. Posocco, M. Fermeglia, L. Vio, S. Pricl, *ACS Med. Chem. Lett.* **2011**, *2*, 834 – 839.

[8] M. Juza, *HPLC Made to Measure—A Practical Handbook for Optimization*, Wiley-VCH, Weinheim, **2006**.

[9] a) A. B. Lemay, K. S. Vulic, W. W. Ogilvie, *J. Org. Chem.* **2006**, *71*, 3615 – 3618; b) J. Simard-Mercier, J. L. Jiang, M. L. Ho, A. B. Flynn, W. W. Ogilvie, *J. Org. Chem.* **2008**, *73*, 5899 – 5906.

[10] D. H. Appella, Y. Moritani, R. Shintani, E. M. Ferreira, S. L. Buchwald, *J. Am. Chem. Soc.* **1999**, *121*, 9473 – 9474.

[11] a) E. Laurini, D. Marson, V. Dal Col, M. Fermeglia, M. G. Mamolo, D. Zampieri, L. Vio, S. Pricl, *Mol. Pharmaceutics* **2012**, *9*, 3107 – 3126; b) C. Meyer, D. Schepmann, S. Yanagisawa, J. Yamaguchi, V. Dal Col, E. Laurini, K. Itami, S. Pricl, B. Wünsch, *J. Med. Chem.* **2012**, *55*, 8047 – 8065; c) P. Seth, M. E. Ganapathy, S. J. Conway, C. D. Bridges, S. B. Smith, P. Casellas, V. Ganapathy, *Biochim. Biophys. Acta Mol. Cell Res.* **2001**, *1540*, 59 – 67.

[12] a) A. Pal, A. R. Hajipour, D. Fontanilla, S. Ramachandran, U. B. Chu, T. Mavlyutov, A. E. Ruoho, *Mol. Pharmacol.* **2007**, *72*, 921 – 933; b) A. Pal, U. B. Chu, S. Ramachandran, D. Grawoig, L. W. Guo, A. R. Hajipour, A. E. Ruoho, *J. Biol. Chem.* **2008**, *283*, 19646 – 19656.

[13] J. Srinivasan, T. E. Cheatham, P. Cieplak, P. A. Kollman, D. A. Case, *J. Am. Chem. Soc.* **1998**, *120*, 9401 – 9409.

[14] a) R. Mancuso, S. Olivan, A. Rando, C. Casas, R. Osta, X. Navarro, *Neurotherapeutics* **2012**, *9*, 814 – 826; b) M. Peviani, E. Salvaneschi, L. Bontempi, A. Petese, D. Rossi, S. Collina, P. Bigini, D. Curti, unpublished results.

[15] D. D. Perrin, W. L. F. Armarego, *Purification of Laboratory Chemicals*, Pergamon, Oxford, **1988**.

[16] a) J. O'Neill, K. S. Yoo, K. W. Jung, *Tetrahedron Lett.* **2008**, *49*, 7307 – 7310; b) A. Gangjee, J. Yang, S. F. Queener, *Bioorg. Med. Chem.* **2006**, *14*, 8341 – 8351.

[17] M. M. Bradford, *Anal. Biochem.* **1976**, *72*, 248 – 254.

[18] C. M. Stoscheck, *Methods Enzymol.* **1990**, *182*, 50 – 68.

[19] Y. Cheng, W. H. Prusoff, *Biochem. Pharmacol.* **1973**, *22*, 3099 – 3108.

[20] a) E. Laurini, D. Zampieri, M. G. Mamolo, L. Vio, C. Zanette, C. Florio, P. Posocco, M. Fermeglia, S. Pricl, *Bioorg. Med. Chem. Lett.* **2010**, *20*, 2954 – 2957; b) M. Mazzei, E. Nieddu, M. Miele, A. Balbi, M. Ferrone, M. Fermeglia, M. T. Mazzei, S. Pricl, P. La Colla, F. Marongiu, C. Ibba, R. Loddo, *Bioorg. Med. Chem.* **2008**, *16*, 2591 – 2605; c) D. Zampieri, M. G. Mamolo, L. Vio, E. Banfi, G. Scialino, M. Fermeglia, M. Ferrone, S. Pricl, *Bioorg. Med. Chem.* **2007**, *15*, 7444 – 7458; d) A. Carta, M. Loriga, G. Paglietti, M. Ferrone, M. Fermeglia, S. Pricl, T. Sanna, C. Ibba, P. La Colla, R. Loddo, *Bioorg. Med. Chem.* **2007**, *15*, 1914 – 1927; e) A. Carta, G. Loriga, S. Piras, G. Paglietti, M. Ferrone, M. Fermeglia, S. Pricl, P. La Colla, B. Secci, G. Collu, R. Loddo, *Med. Chem.* **2006**, *2*, 577 – 589; f) V. Frecer, M. Kabeláč, P. De Nardi, S. Pricl, S. Miertuš, *J. Mol. Graphics Modell.* **2004**, *22*, 209 – 220.

[21] D. A. Case, T. A. Darden, T. E. Cheatham III, C. L. Simmerling, J. Wang, R. E. Duke, R. Luo, R. C. Walker, W. Zhang, K. M. Merz, B. Roberts, B. Wang, S. Hayik, A. Roitberg, G. Seabra, I. Kolossváry, K. F. Wong, F. Paesani, J. Vanicek, X. Wu, S. R. Brozell, T. Steinbrecher, H. Gohlke, Q. Y. Cai, X., J. Wang, M.-J. Hsieh, G. Cui, D. R. Roe, D. H. Mathews, M. G. Seetin, C. Sagui, V. Babin, T. Luchko, S. Gusarov, A. Kovalenko, P. A. Kollman, *AMBER 11*, University of California, San Francisco, **2010**.

[22] a) C. I. Bayly, P. Cieplak, W. D. Cornell, P. A. Kollman, *J. Phys. Chem.* **1993**, *97*, 10269 – 10280; b) W. D. Cornell, P. Cieplak, C. I. Bayly, P. A. Kollman, *J. Am. Chem. Soc.* **1993**, *115*, 9620 – 9631; c) P. Cieplak, W. D. Cornell, C. Bayly, P. A. Kollman, *J. Comput. Chem.* **1995**, *16*, 1357 – 1377.

[23] a) U. C. Singh, P. A. Kollman, *J. Comput. Chem.* **1984**, *5*, 129 – 145; b) B. H. Besler, K. M. Merz, P. A. Kollman, *J. Comput. Chem.* **1990**, *11*, 431 – 439.

[24] Y. Duan, C. Wu, S. Chowdhury, M. C. Lee, G. M. Xiong, W. Zhang, R. Yang, P. Cieplak, R. Luo, T. Lee, J. Caldwell, J. M. Wang, P. Kollman, *J. Comput. Chem.* **2003**, *24*, 1999 – 2012.

[25] J. Wang, R. M. Wolf, J. W. Caldwell, P. A. Kollman, D. A. Case, *J. Comput. Chem.* **2004**, *25*, 1157 – 1174.

[26] a) A. Carta, I. Briguglio, S. Piras, G. Boatto, P. La Colla, R. Loddo, M. Tolomeo, S. Grimaudo, A. Di Cristina, R. M. Pipitone, E. Laurini, M. S. Paneni, P. Posocco, M. Fermeglia, S. Pricl, *Eur. J. Med. Chem.* **2011**, *46*, 4151 – 4167; b) X. J. Liu, H. Chen, E. Laurini, Y. Wang, V. Dal Col, P. Posocco, F. Ziarelli, M. Fermeglia, C. C. Zhang, S. Pricl, L. Peng, *Org. Lett.* **2011**, *13*, 2924 – 2927; c) G. Giliberti, C. Ibba, E. Marongiu, R. Loddo, M. Tonelli, V. Boido, E. Laurini, P. Posocco, M. Fermeglia, S. Pricl, *Bioorg. Med. Chem.* **2010**, *18*, 6055 – 6068; d) M. Tonelli, V. Boido, P. La Colla, R. Loddo, P. Posocco, M. S. Paneni, M. Fermeglia, S. Pricl, *Bioorg. Med. Chem.* **2010**, *18*, 2304 – 2316; e) A. Carta, S. Pricl, S. Piras, M. Fermeglia, P. La Colla, R. Loddo, *Eur. J. Med. Chem.* **2009**, *44*, 5117 – 5122; f) M. Tonelli, I. Vazzana, B. Tasso, V. Boido, F. Sparatore, M. Fermeglia, M. S. Paneni, P. Posocco, S. Pricl, P. La Colla, C. Ibba, B. Secci, G. Collu, R. Loddo, *Bioorg. Med. Chem.* **2009**, *17*, 4425 – 4440.

[27] G. M. Morris, R. Huey, W. Lindstrom, M. F. Sanner, R. K. Belew, D. S. Goodsell, A. J. Olson, *J. Comput. Chem.* **2009**, *30*, 2785 – 2791.

[28] E. L. Mehler, T. Solmajer, *Protein Eng.* **1991**, *4*, 903 – 910.

[29] a) A. Onufriev, D. Bashford, D. A. Case, *J. Phys. Chem. B* **2000**, *104*, 3712 – 3720; b) M. Feig, A. Onufriev, M. S. Lee, W. Im, D. A. Case, C. L. Brooks, *J. Comput. Chem.* **2004**, *25*, 265 – 284.

[30] W. L. Jorgensen, J. Chandrasekhar, J. D. Madura, R. W. Impey, M. L. Klein, *J. Chem. Phys.* **1983**, *79*, 926 – 935.

[31] J. P. Ryckaert, G. Ciccotti, H. J. C. Berendsen, *J. Comput. Phys.* **1977**, *23*, 327 – 341.

[32] A. Toukmaji, C. Sagui, J. Board, T. Darden, *J. Chem. Phys.* **2000**, *113*, 10913 – 10927.

[33] a) P. Posocco, E. Laurini, V. Dal Col, D. Marson, K. Karatasos, M. Fermeglia, S. Pricl, *Curr. Med. Chem.* **2012**, *19*, 5062 – 5087; b) X. Liu, C. Liu, E. Laurini, P. Posocco, S. Pricl, F. Qu, P. Rocchi, L. Peng, *Mol. Pharmaceutics* **2012**, *9*, 470 – 481; c) K. Karatasos, P. Posocco, E. Laurini, S. Pricl, *Macromol. Biosci.* **2012**, *12*, 225 – 240; d) D. L. Gibbons, S. Pricl, H. Kantarjian, J. Cortes, A. Quintas-Cardama, *Cancer* **2012**, *118*, 293 – 299; e) X. Liu, J. Wu, M. Yammine, J. Zhou, P. Posocco, S. Viel, C. Liu, F. Ziarelli, M. Fermeglia, S. Pricl, G. Victorero, C. Nguyen, P. Erbacher, J. P. Behr, L. Peng, *Bioconjugate Chem.* **2011**, *22*, 2461 – 2473; f) A. Barnard, P. Posocco, S. Pricl, M. Calderon, R. Haag, M. E. Hwang, V. W. Shum, D. W. Pack, D. K. Smith, *J. Am. Chem. Soc.* **2011**, *133*, 20288 – 20300; g) M. A. Pierotti, E. Tamborini, T. Negri, S. Pricl, S. Pilotti, *Nat. Rev. Clin. Oncol.* **2011**, *8*, 161 – 170; h) P. Dileo, S. Pricl, E. Tamborini, T. Negri, S. Stacchiotti, A. Gronchi, P. Posocco, E. Laurini, P. Coco, E. Fumagalli, P. G. Casali, S. Pilotti, *Int. J. Cancer* **2011**, *128*, 983 – 990; i) G. M. Pavan, P. Posocco, A. Tagliabue, M. Maly, A. Malek, A. Danani, E. Ragg, C. V. Catapano, S. Pricl, *Chem. Eur. J.* **2010**, *16*, 7781 – 7795; j) S. P. Jones, G. M. Pavan, A. Danani, S. Pricl, D. K. Smith, *Chem. Eur. J.* **2010**, *16*, 4519 – 4532; k) M. A. Pierotti, T. Negri, E. Tamborini, F. Perrone, S. Pricl, S. Pilotti, *Mol. Oncol.* **2010**, *4*, 19 – 37; l) E. Conca, T. Negri, A. Gronchi, E. Fumagalli, E. Tamborini, G. M. Pavan, M. Fermeglia, M. A. Pierotti, S. Pricl, S. Pilotti, *Mol. Cancer Ther.* **2009**, *8*, 2491 – 2495.

[34] M. K. Gilson, K. A. Sharp, B. H. Honig, *J. Comput. Chem.* **1988**, *9*, 327 – 335.

[35] D. Sitkoff, K. A. Sharp, B. Honig, *J. Phys. Chem.* **1994**, *98*, 1978 – 1988.

[36] M. F. Sanner, A. J. Olson, J. C. Spehner, *Biopolymers* **1996**, *38*, 305 – 320.

[37] E. B. Wilson, J. C. Decius, P. C. Cross, *Molecular Vibrations*, McGraw-Hill, New York, **1995**.

[38] modeFRONTIER, Esteco SpA: http://esteco.com/modefrontier (accessed June 19, 2013).

[39] E. Meijering, M. Jacob, J. C. F. Sarria, P. Steiner, H. Hirling, M. Unser, *Cytometry Part A* **2004**, *58A*, 167 – 176.

Received: May 16, 2013
Published online on July 5, 2013